Molecular Therapy
Original Article

AAV-Mediated Progranulin Delivery to a Mouse Model of Progranulin Deficiency Causes T Cell-Mediated Toxicity

Defne A. Amado,[1,4] Julianne M. Rieders,[2,3,4] Fortunay Diatta,[1] Pilar Hernandez-Con,[1] Adina Singer,[1] Jordan T. Mak,[1] Junxian Zhang,[1] Eric Lancaster,[1] Beverly L. Davidson,[2,3] and Alice S. Chen-Plotkin[1]

[1]Department of Neurology, Perelman School of Medicine, University of Pennsylvania, Philadelphia, PA 19104, USA; [2]Department of Pathology and Laboratory Medicine, University of Pennsylvania, Philadelphia, PA 19104, USA; [3]Children's Hospital of Philadelphia, 3501 Civic Center Boulevard, 5060 CTRB, Philadelphia, PA 19104, USA

Adeno-associated virus-mediated gene replacement is emerging as a safe and effective means of correcting single-gene mutations affecting the CNS. AAV-mediated progranulin gene (*GRN*) delivery has been proposed as a treatment for *GRN*-deficient frontotemporal dementia and neuronal ceroid lipofuscinosis, and recent studies using intraparenchymal AAV-*Grn* delivery to brain have shown moderate success in histopathologic and behavioral rescue in mouse models. Here, we used AAV9 to deliver *GRN* to the lateral ventricle to achieve widespread expression in the *Grn* null mouse brain. We found that, despite a global increase in progranulin, overexpression resulted in dramatic and selective hippocampal toxicity and degeneration affecting neurons and glia. Hippocampal degeneration was preceded by T cell infiltration and perivascular cuffing. *GRN* delivery with an ependymal-targeting AAV for selective secretion of progranulin into the cerebrospinal fluid similarly resulted in T cell infiltration, as well as ependymal hypertrophy. Interestingly, overexpression of *GRN* in wild-type animals also provoked T cell infiltration. These results call into question the safety of *GRN* overexpression in the CNS, with evidence for both a region-selective immune response and cellular proliferative response. Our results highlight the importance of careful consideration of target gene biology and cellular response to overexpression prior to progressing to the clinic.

INTRODUCTION

Frontotemporal dementia (FTD)[1,2] and neuronal ceroid lipofuscinosis (NCL) type 11 (CLN11)[3] are neurodegenerative diseases resulting from haploinsufficiency or complete deficiency of progranulin (GRN), encoded by the gene *GRN*. FTD symptoms range from behavioral changes to language deterioration, with death ensuing in 3–5 years.[4] Nearly 70 FTD-causing *GRN* mutations have been identified, accounting for up to 25% of inherited cases, >90% of which are nonsense mutations.[1,2,5] For poorly understood reasons, *GRN* deficiency results in the accumulation of Tar-DNA binding protein of 43 kDa (TDP-43)[1,2] in characteristic inclusion bodies, with subsequent neuronal loss and atrophy of frontal and temporal lobes. In CLN11, complete *GRN* deficiency leads to lysosomal dysfunction and accumulation of lipofuscin, as well as a clinical syndrome of generalized seizures, cognitive dysfunction, vision loss, and cerebellar degeneration.[6–8] Strategies to boost GRN have been under development since its discovery as a major causal mutation for these diseases.[9–11]

GRN is a secreted growth factor involved in development, wound healing, and immune modulation.[12,13] In mice, *Grn* is expressed highly in neurons and is upregulated in activated microglia following injury.[14] In human postmortem brain, GRN expression is widespread in both normal and FTD subjects.[15] *In vitro* and *in vivo*, GRN plays a role in neuronal survival and neurite outgrowth,[16–18] and a neuronal GRN receptor, sortilin, has been identified.[19] Based on its growth-promoting properties, GRN augmentation has been considered for treatment of a range of neurodegenerative diseases. Indeed, lentivirus- and adeno-associated virus (AAV)-mediated *GRN* delivery to the CNS has been investigated in preclinical models of Alzheimer's disease,[20,21] Parkinson's disease,[22] motor neuron disease,[23,24] and Huntington's disease.[25]

Methods to augment *GRN* expression include enhancing transcription[10] or translation,[9] increasing extracellular GRN levels,[11] or using gene therapy. Among the latter, gene delivery using AAV vectors has risen to the forefront based on its excellent safety and efficacy profile, and it has been used in preclinical models of diverse diseases for several decades. Recent successes in humans include treatment of hemophilia, Leber's congenital amaurosis, and spinal muscular atrophy.[26–28] To transduce the CNS, AAV can be delivered to brain

Received 23 May 2018; accepted 11 November 2018;
https://doi.org/10.1016/j.ymthe.2018.11.013.

[4]These authors contributed equally to this work.

Correspondence: Beverly L. Davidson, PhD, Children's Hospital of Philadelphia, 3501 Civic Center Boulevard, 5060 CTRB, Philadelphia, PA 19104, USA.
E-mail: davidsonbl@email.chop.edu
Correspondence: Alice S. Chen-Plotkin, MD, Department of Neurology, Perelman School of Medicine, University of Pennsylvania, 3 W Gates, 3400 Spruce Street, Philadelphia, PA 19104, USA.
E-mail: chenplot@pennmedicine.upenn.edu

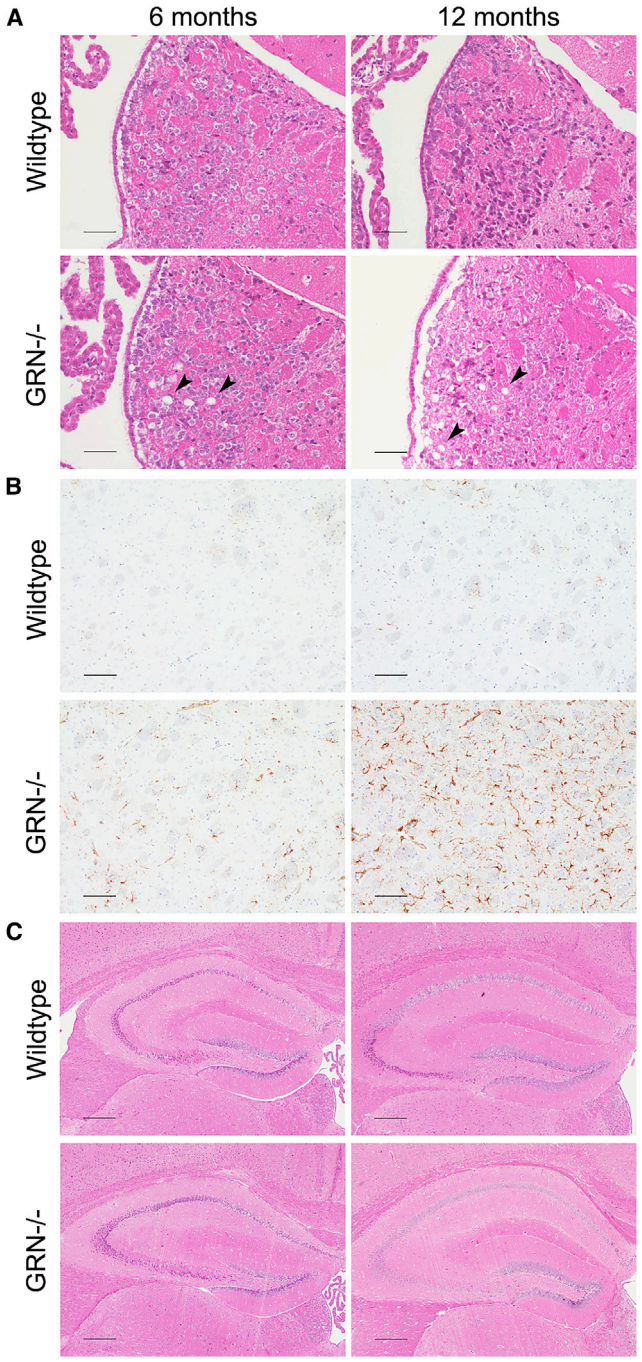

Figure 1. *Grn* Null Mice Recapitulate Previously Published Histopathologic Findings and Exhibit Previously Undescribed Abnormalities

(A) *Grn* null mice exhibit vacuolation that is most pronounced in the habenula and increases with age (arrowheads) and is absent from WT mice at all time points. (Scale bars: 50 μm.) (B) *Grn* null mice demonstrate an age-dependent increase in astrocytosis compared to WT mice, as seen by GFAP staining. Indicated here is the striatum, an area in which astrocytosis in *Grn* null mice has not been previously described. (Scale bars: 100 μm.) (C) The hippocampus shows no gross morphological differences in *Grn* null mice compared to WT at 6 or 12 months. (Scale bars: 250 μm.)

parenchyma or cerebrospinal fluid (CSF), with therapeutic benefit in preclinical models of both gain- and loss-of-function diseases.[29–34] In contrast to peripheral administration,[35,36] numerous studies have shown minimal innate or adaptive immune response to AAV-mediated gene delivery in the CNS.

A recent study using bilateral injection of AAV1.*Grn* into the medial prefrontal cortex of *Grn* null mice demonstrated focal improvements in lipofuscinosis, microgliosis, and lysosomal function.[37] This group had previously used this approach in *Grn* haploinsufficient mice and showed improvement in lysosomal readouts and social dominance deficits.[38] Notably, *Grn* null mice displayed microglial activation at the injection site, with induction of anti-GRN antibodies.[37] No other immunologic phenotypes were reported in this short-term study.

While these studies are promising, translation of intraparenchymal gene delivery to the human brain is challenging. Our aim was to deliver *GRN* globally and sustainably using a method easily translatable to humans; namely, a single intraventricular injection of AAV.*GRN*. We selected AAV serotype 9 (AAV9) based on its ability to broadly disperse and infect neurons and glia after CSF delivery, as well as its prior track record.[28,34,39] We also tested AAV serotype 4 (AAV4), due to its ependymal selectivity and safety profile,[30,40,41] to maximize CSF secretion with the goal of broad CNS uptake through the sortilin receptor. Regardless of serotype, our studies show that overexpression of *GRN* in brain is deleterious, causing profound neurodegeneration and raising concern about excessive expression of *GRN* in mammalian brain as a therapy for FTD and/or NCL.

RESULTS

Characterization of the *Grn* Null Phenotype

As *Grn* haploinsufficient mice have minimal phenotypes, we used *Grn* null mice for our studies. Mice lacking *Grn* have an age-dependent histopathologic phenotype consisting of habenular and hippocampal vacuolation and increased ubiquitination starting at 7 months of age, as well as diffusely increased astrogliosis and microgliosis starting at 12 months of age.[42–44] In our *Grn* null animals, we confirmed the previously reported increase in vacuolation,[42] which was most pronounced in the habenula and increased with age (Figure 1A, arrowheads). Additionally, we noted astrocytosis in the *Grn* null striatum that is present as early as 6 months and progresses with age; this histopathological finding was not present, even in 12-month-old wild-type (WT) mice (Figure 1B), and has not been previously described. Hippocampal morphology was unaffected by genotype at any age (Figure 1C).

AAV-Mediated Gene Transfer Results in Sustained GRN Expression in *Grn* Null Mice

Grn null mice were injected with AAV9 encoding human *GRN* (AAV9.*GRN*) (Figure S1) in the right posterior lateral ventricle at 6–7.5 months of age and sacrificed at time points ranging from 1 to 6 months post-injection. We observed the highest levels of GRN expression, as detected by ELISA, in the ipsilateral periventricular region; GRN levels remained undiminished at 1, 3, 4.5, and 6 months

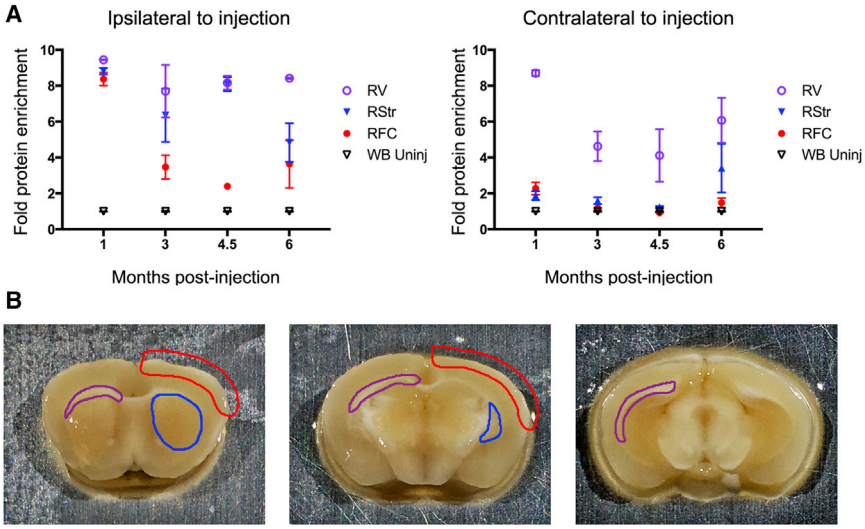

Figure 2. AAV9 Mediates Sustained Expression of GRN in *Grn* Null Mouse Brain

Grn null mice were injected at 6–7.5 months of age with AAV9.*GRN* or AAV9.*eGFP* in the right lateral ventricle and sacrificed 1, 3, 4.5, or 6 months post-injection. Brains were microdissected, and GRN levels were measured by ELISA. (A) Left: GRN levels remained elevated at all time points in the right (injected) peri-ventricular area (RV), right striatum (RStr), and right frontal cortex (RFC) as compared to uninjected homogenized whole brain (WB). (A) Right: GRN levels remained elevated at all time points in the left (uninjected) peri-ventricular area (LV), but far less so in the left striatum (LStr) and left frontal cortex (LFC) as compared to uninjected homogenized whole brain (WB). (B) Schematic illustrating the regions collected by microdissection in blue (striatum), red (cortex), and purple (periventricular area). n = 3 mice per group at each time point.

post-injection, compared to levels in uninjected whole brain tissue from null mice (Figure 2A, left). We also observed high GRN levels in the ipsilateral striatum and, to a lesser extent, the ipsilateral frontal cortex, although cortical expression diminished over time. Similarly high levels of GRN were detected in the contralateral periventricular region (Figure 2A, right) but with minimal increase in the left striatum or left frontal cortex. GRN was additionally detected at moderate levels in the periventricular region of the third ventricle, the brainstem, and the spinal cord at all time points (Figure S2). These data indicate broad, sustained *GRN* expression.

AAV9-Mediated Overexpression of *GRN* Causes Progressive Hippocampal Toxicity

Having established sustained expression of *GRN*, we next performed detailed histological and immunohistochemical analyses to assess for rescue in our treated mice. *Grn* null animals injected with AAV9.*GRN* at 6–7.5 months of age and sacrificed 6 months after injection had striking morphological and histological changes in the hemisphere ipsilateral to injection. Specifically, in 10 out of 10 injected animals, the hippocampus ipsilateral to the injection site showed a hypercellular infiltrate often accompanied by loss of structural integrity (Figure 3A). In all cases, adjacent structures, as well as the contralateral hippocampus, appeared relatively unaffected. Similar hippocampal degeneration occurred in *Grn* null mice injected with an AAV9 vector delivering mouse *Grn* (Figure S3), indicating that the response was not specific to delivery of a human gene.

To better define the timeline of degenerative changes, animals were harvested soon after injection. At 1 month post-injection with AAV9.*GRN*, a hypercellular infiltrate was noted to extend anteriorly and posteriorly along the entire hippocampus (Figure 3B, left panels) and was most prominent inferior to and within the hippocampal parenchyma. By 6 months post-injection, prominent hypercellular infiltrates and perivascular cuffing accompanied loss of recognizable hippocampal structures (Figure 3B, right panels), and staining confirmed strong GRN expression in these regions (Figure 3C). Positive GRN staining was noted in neurons that appeared to be healthy (Figure 3C, lower inset) and in cells with pyknotic nuclei (Figure 3C, arrow). In contrast, littermate control animals treated with AAV9-delivered *eGFP* (AAV9.*eGFP*) showed no pathology at 6 months post-injection (Figure 3D) and appeared similar to uninjected littermates (data not shown), despite high levels of EGFP expression.

Indeed, over 4 time points after injection, in histopathological assessments performed by observers blinded to treatment condition, 17/17 (100%) of the AAV9.*GRN*-injected animals showed evidence of hippocampal toxicity, with 10/17 (59%) affected severely enough to cause atrophy visible to the naked eye. In contrast, 0/18 (0%) of the AAV9.*eGFP*-injected animals exhibited evidence of toxicity (Figure 3E).

Responses to *hGRN* Overexpression Are Region- and Cell-Type Specific

Histological assessments were performed to determine whether the hypercellular infiltrates and degeneration observed after AAV9.*GRN* delivery were present in other brain regions with high levels of expression. No differences were seen between the cortex ipsilateral to the injection site and either the contralateral cortex or that of AAV9.*eGFP*-injected controls at 6 months post-injection (Figures 4A and 4B), despite moderately high GRN levels in cortical brain isolates (Figure 2). Indeed, cortical neuron organization remained intact ipsilateral to the site of AAV9.*GRN* injection (Figure 4C), and no obvious changes in architecture, neuronal number, or gliosis were found in the ipsilateral striatum (Figures 4D–4G), an area with high GRN levels (Figure 2). Brain tissue samples from AAV9.*eGFP*-injected animals and from uninjected animals were similar in appearance across all parameters (data not shown). These results suggest that *GRN* overexpression selectively affects hippocampal brain regions.

To determine what cell types were affected in the hippocampus anteriorly (Figures 5A–5D) and posteriorly (Figures 5E–5H), tissue

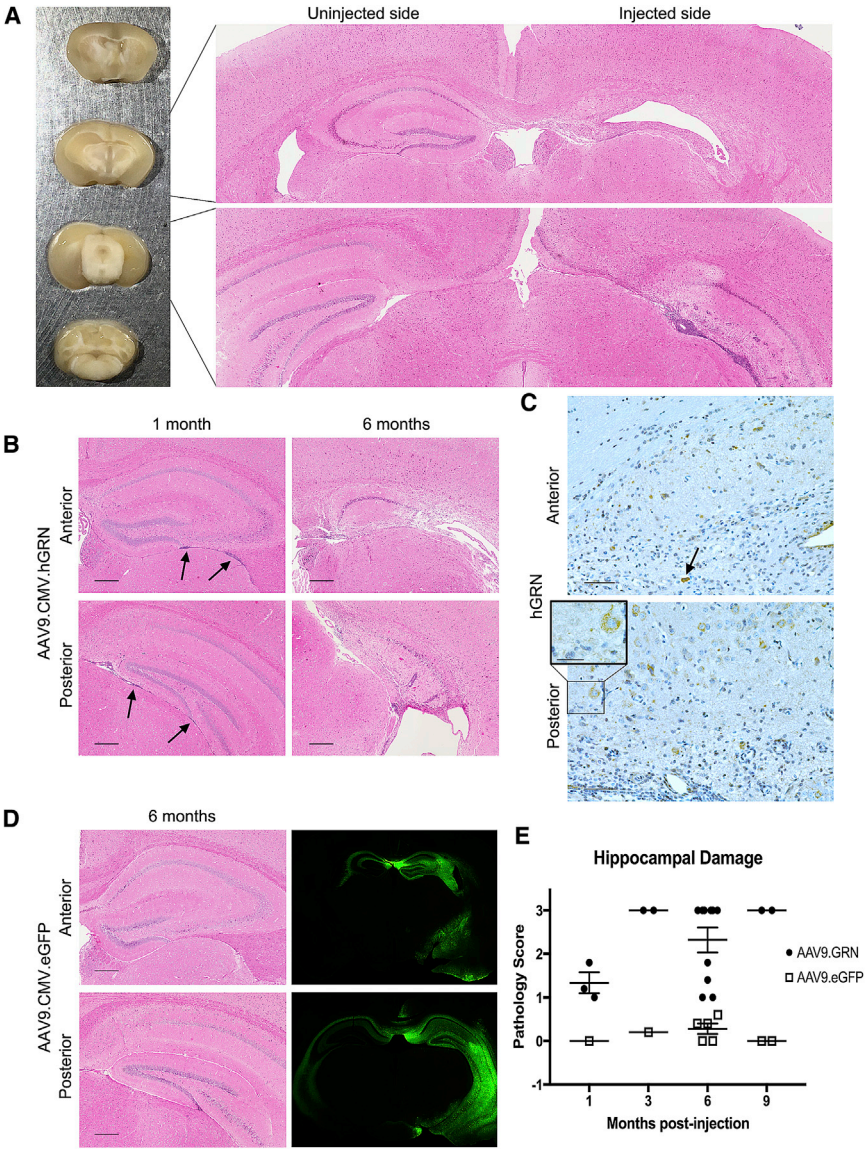

Figure 3. Overexpression of GRN Is Toxic to Cells of the Hippocampus

Mice were injected at 6–8 months of age and sacrificed 1–9 months post-injection, and brains were either embedded and stained for immunohistochemical analysis (A–E) or sectioned and imaged fluoroscopically (D). (A) Left: histological differences were observed between the injected and uninjected hemispheres in 10 of 10 mice 6 months after injection of AAV9.*GRN*, in 6 of whom there was grossly visible atrophy of the hippocampus on the injected side. Right: H&E of AAV9.*GRN*-injected mouse brain revealed marked degeneration of the hippocampus ipsilateral to injection and a dense cellular infiltrate throughout the remaining hippocampal tissue, extending from anterior (upper panel) to posterior (lower panel). (B) The cellular infiltrate was observed along the length of the hippocampus as early as 1 month post-injection of AAV9.*GRN*, both inferior to (arrows) and within the parenchyma of the hippocampus (left panels; n = 3 mice). By 6 months, histological changes were observed in 10 of 10 mice, with 6 of 10 showing pervasive cell loss (right panels). (Scale bars: 250 μm.) (C) High levels of GRN were detected throughout the hippocampus at all time points, with a diffuse cytoplasmic pattern of expression (inset). In some cases, cells expressing GRN exhibited pyknotic nuclei (arrow). Indicated here is GRN expression 6 months post-injection. (Scale bars: 50 μm; inset: 25 μm.) (D) Left panels: AAV9.*eGFP*-injected brains did not display cell loss or hypercellular infiltrate at 1 (n = 3), 3 (n = 6), 6 (n = 5), and 9 (n = 4) months post-injection and were similar in appearance to those of uninjected *Grn* null mice (n = 4 age-matched littermates to 6-month cohort; data not shown). Expression 6 months post-injection is indicated here. (Scale bars, 250 μm.) (D) Right panels: high levels of EGFP expression were detected by fluorescence microscopy adjacent to the injection site, with cross-over to the contralateral side. Expression 3 months post-AAV9.*eGFP* injection is indicated here. (E) Quantitative assessment of hippocampal toxicity by raters blinded to treatment condition showed toxicity ranging from hypercellular infiltrates to pervasive cell loss in 17/17 (100%) of AAV9.*GRN*-treated animals, compared to 0/18 (0%) of AAV9.*eGFP*-treated animals. Data are presented as mean ± SEM.

sections were stained for the neuronal marker NeuN, the glial marker glial fibrillary acidic protein (GFAP), and the microglial marker Iba-1. In 13/17 (76%) of AAV9.*GRN*-injected mice, hippocampal neuronal loss was noted (Figures 5B and 5F). Hippocampal astrocytes demonstrated fewer, less robust processes (Figures 5C and 5G), and microglial infiltration ipsilateral to the injection was prominent (Figures 5D and 5H).[45] In all cases, the side contralateral to the injection (left panels) appeared similar to the hippocampus of both AAV9.*eGFP*-injected and uninjected control littermates (data not shown). These data indicate that AAV9-mediated *GRN* overexpression is toxic to neurons and astrocytes in the hippocampus and provokes a strong local microglial response.

A T Cell-Mediated Inflammatory Response Precedes Neuronal Loss and Occurs in Both WT and *Grn* Null Animals

The hypercellular infiltrate found in AAV9.*GRN*-injected animals consisted of cells with a high nucleus-to-cytoplasm ratio characteristic of lymphocytes. As such, sections were stained for the cell proliferation marker Ki-67, the B lymphocyte marker B220 (CD45), and the T lymphocyte marker CD3.

As shown in Figure 6, abundant proliferative cells were noted (Figures 6B and 6F), and the majority of these cells were positive for CD3 (Figures 6C and 6G). In both anterior and posterior sections, there was extensive perivascular cuffing by CD3+ cells

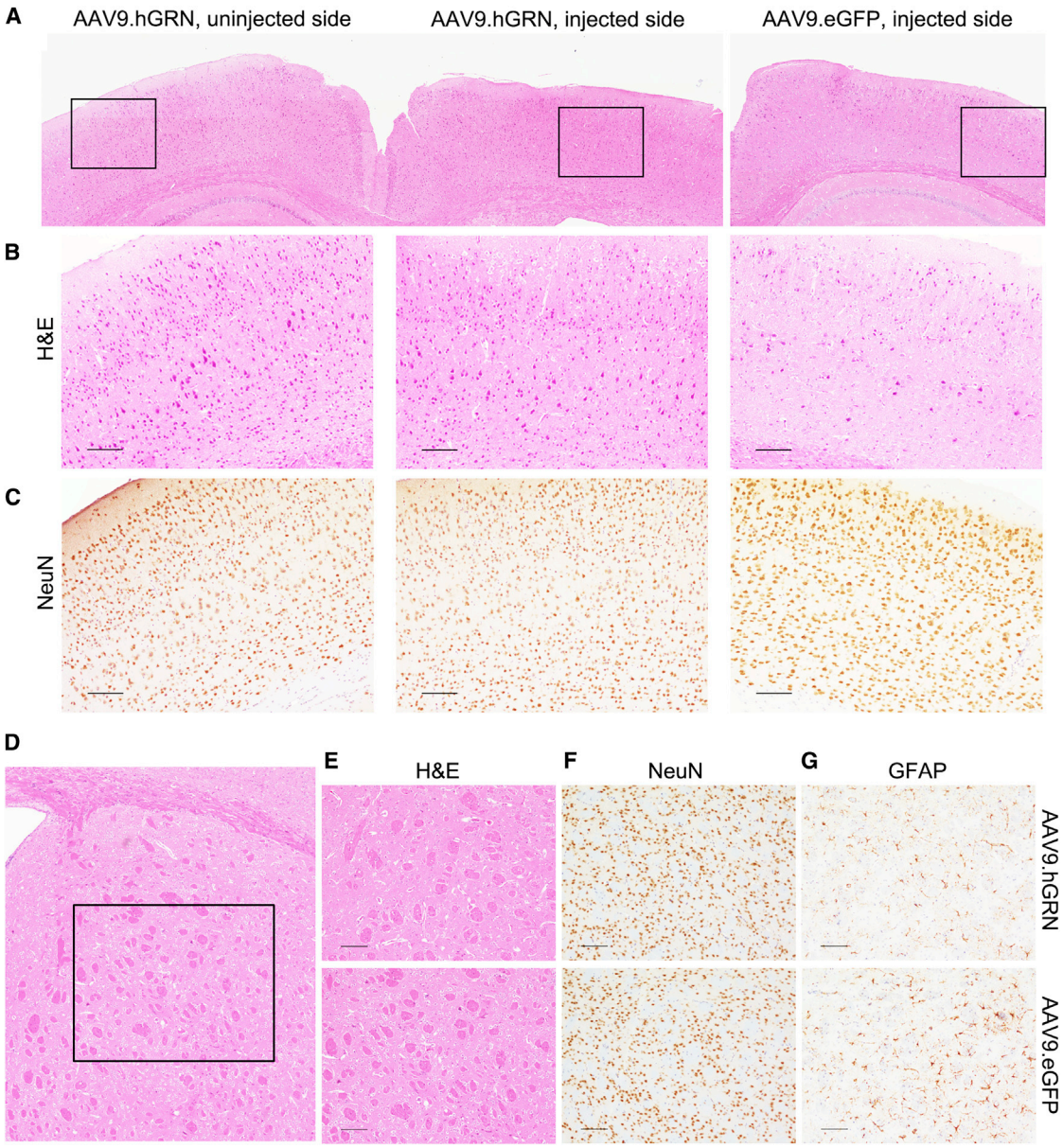

Figure 4. The Cortex and Striatum Are Unaffected by GRN Overexpression

(A) The ipsilateral cortex immediately adjacent to the degenerated hippocampus appeared unaffected by AAV9.*GRN* overexpression when compared to the contralateral cortex and to cortex ipsilateral to AAV9.*eGFP*-injected brain. Gross morphology, layer organization, and neuronal numbers appeared unremarkable by H&E staining (B; n = 10 AAV9.*GRN*-injected mice, and n = 5 AAV9.*eGFP*-injected mice assessed); NeuN staining confirmed intact neuronal appearance (C). (Scale bars: 100 μm.) Similarly, the ipsilateral striatum directly anterior to the degenerated hippocampus (D) appeared unremarkable by H&E (E), NeuN (F), and GFAP (G) staining, compared to AAV9.*eGFP*-injected controls 6 months post-injection (scale bars: 100 μm), as well as to uninjected controls (data not shown).

both within and adjacent to the hippocampus (Figure 6G, arrowheads). These data collectively indicate a robust T cell infiltration of the hippocampal region, with minimal contribution from B cells.

To test whether inflammatory infiltrates precede or follow the hippocampal degeneration, brain sections from animals sacrificed at earlier time points after AAV9.*GRN* injection were characterized. At 1 month post-injection, hippocampal structures were maintained, despite dense cellular infiltration ventral to the hippocampus, with widespread perivascular cuffing lateral to and within the hippocampus (Figure 6I). Infiltrating cells were positive for CD3 and negative for B220, indicating that T cell infiltration precedes hippocampal neurodegeneration.

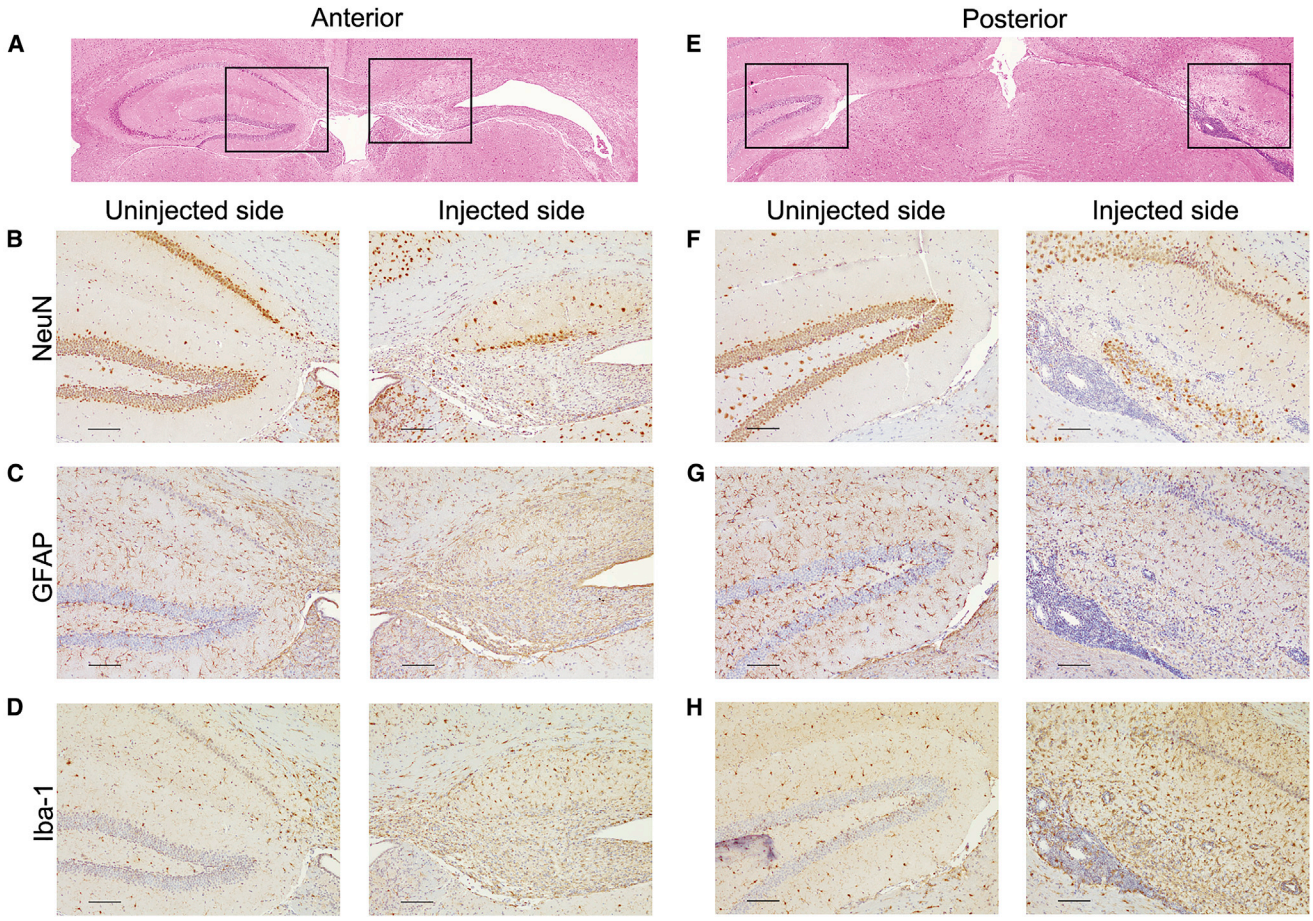

Figure 5. AAV9.*GRN*-Overexpressing Mice Undergo Cell-Specific Hippocampal Degeneration

H&E-stained coronal sections indicated hippocampal degeneration 6 months post-injection on the injected side anteriorly (A) and posteriorly (E), with boxes indicating regions that are magnified below, in (B)–(D) and (F)–(H). On the injected side, NeuN staining indicated striking neuronal loss throughout all regions of the hippocampus both anteriorly (B) and posteriorly (F); GFAP staining showed qualitative loss of astrocytic processes in anterior (C) and posterior (G) hippocampus; and Iba-1 staining for microglia showed a dense microglial infiltrate in the hippocampal region anteriorly (D) and posteriorly (H). Throughout the hippocampus, there was a dense cellular infiltrate in the ependymal space underlying the hippocampus (F–H) ipsilateral to injection. (Scale bars: 100 μm.)

In human autoimmune encephalitides, hippocampal degeneration often ensues from autoantibodies specific for hippocampal antigens. Triggering events may be the expression of an ectopic antigenic protein by a tumor or the unmasking of a native hippocampal antigen by an inflammatory process.[46] Therefore, we tested whether *GRN* overexpression elicited a similar pathophysiological process in our *Grn* null animals using a previously described rat hippocampal slice assay.[47] As shown in Figure 6J, serum from mice with the hippocampal degeneration phenotype screened negative for anti-hippocampal antibodies, regardless of whether serum was drawn 1, 3, or 6 months after AAV9.*GRN* injection. Moreover, AAV9.*GRN* intraventricular delivery into WT animals also elicited perivascular cuffing with infiltration of CD3+ T cells as early as 1 month after gene delivery, which became prominent and was accompanied by loss of hippocampal structures by 3 months post-injection (Figure 7). Taken together, these data support a role for T cell-mediated hippocampal neurodegeneration following *GRN* overexpression.

hGRN Delivered by the AAV4 Ependymal-Targeting Vector Elicits an Inflammatory Response and Ependymal Hypertrophy

AAV9 transduces multiple cell types, including neurons and glia.[48] Therefore, we asked whether the observed inflammatory response and subsequent hippocampal degeneration were serotype specific. For this, we used AAV4, an ependymal-targeting serotype[49] that allows secretion of transgene products into the CSF.[30,41,50] In *Grn* null mice injected at 6.5–8 months with AAV4.*GRN* in the right lateral ventricle, at the same dose as our AAV9.*GRN*-injected animals, GRN was detected throughout the brain by ELISA at mildly increased levels that were greatest in ependyma-rich areas (Figure S4A). A hypercellular infiltrate was present throughout the ventricular system as early as 1 month post-injection (Figure 8A). This infiltrate was not

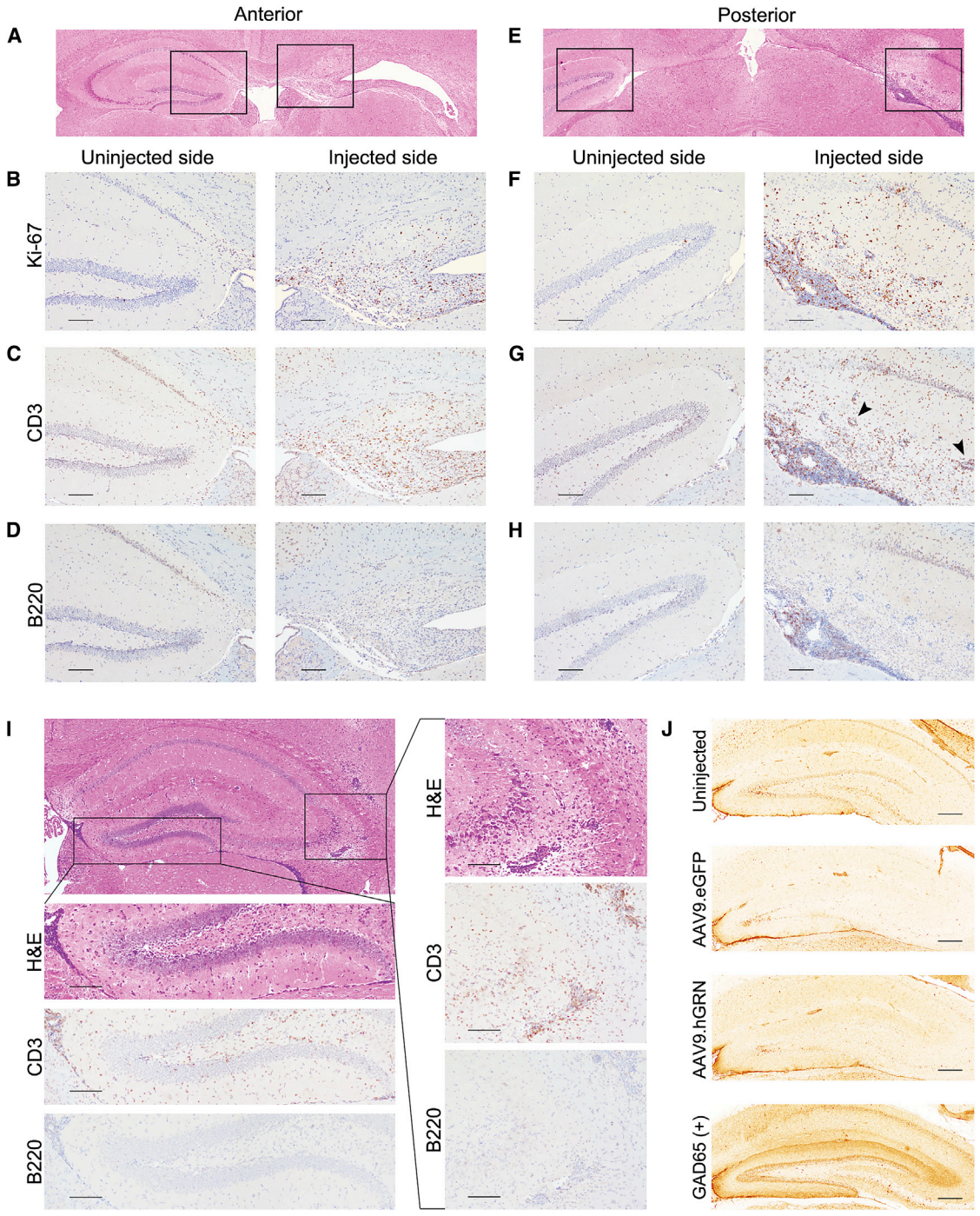

Figure 6. Hippocampal Degeneration Is Characterized by a T Cell Inflammatory Response that Precedes Cell Death

Mice were injected with AAV9.*GRN* at 6–8 months of age and sacrificed 6 months post-injection (A-H) or 1 month post-injection (I). H&E-stained coronal sections indicated hippocampal degeneration 6 months post-injection on the injected side anteriorly (A) and posteriorly (E), with boxes indicating regions magnified below, in (B)–(D) and (F)–(H). On the injected side, Ki-67 staining demonstrated proliferating cells throughout the hippocampus anteriorly (B) and posteriorly (F); CD3 staining identified most of these proliferating cells as T cells (anterior in C and posterior in G), while B220 staining for B cells was largely negative (anterior in D and posterior in H), aside from some positively stained cells in the dense posterior sub-hippocampal infiltrate (H). (Scale bars: 100 μm.) Mice were then examined at 1 month post-injection (I). H&E staining showed a dense infiltrate in the ependymal space inferior to the hippocampus that was CD3+ and B220− (left box and magnifications below; scale bars: 100 μm). In the CA2/3 region, there

(legend continued on next page)

present in AAV4.*eGFP*-injected controls. Consistent with our previous findings, infiltrating cells were positive for the T cell marker CD3 (Figure 8A, right panels).

There was also marked ependymal and choroidal hypertrophy in the lateral ventricles adjacent to the hippocampus (Figure 8B, upper panel), as well as the third ventricle (Figure 8C, upper panel), with corresponding T cell infiltration. By 3 months post-injection, the effect was so severe as to have ablated the lateral ventricles (Figure 8B, lower panel), with choroidal hypertrophy nearly ablating the third ventricle as well (Figure 8C, lower panel). This effect was not seen in AAV4.*eGFP*-injected mice at any time point (Figures 8B and 8C), suggesting a direct effect of GRN-induced cellular proliferation. Additionally, ependymal and choroidal hypertrophy were not observed with AAV9-mediated gene delivery at any time (Figures 8B and 8C). As AAV9 does not efficiently transduce ependymal cells, these data indicate a hypertrophic effect on *GRN* transduced ependymal cells. Of note, the hippocampus was unaffected in AAV4.*GRN*-treated mice, and GRN was not detected in this area (Figure S4B).

To test whether this is an effect of overexpression of transgenes in animals null for a disease gene, we subsequently examined brain sections from mucopolysaccharidosis type IIIA (MPS IIIA) sulfamidase (SGSH) homozygous knockout mice treated with AAV4 expressing human SGSH, a secreted protein, using the same dose, injection coordinates, and volume as in our AAV4.*GRN* studies.[51] There was no observed toxicity in treated MPS IIIA mice (data not shown), supporting an effect specific to GRN.

Cumulatively (Table S1), our data show that overexpression of progranulin in the brain can trigger robust responses in the CNS that, in turn, can cause cellular damage, regardless of the AAV serotype used for delivery.

DISCUSSION

In these studies we sought to test the safety and efficacy of AAV-mediated *GRN* expression in a *Grn* null mouse model, toward the development of a gene replacement strategy for treatment of *GRN*-deficient FTD and CLN11. To our surprise, we found that AAV9-mediated *GRN* or *Grn* overexpression led to hippocampal toxicity in 100% of *Grn* null mice, with hippocampal neurodegeneration in nearly all, while AAV9-mediated *eGFP* overexpression had no deleterious effect. The observed degeneration was markedly selective, with sparing of the cortex above, striatum anterior to, and thalamic structures inferior to the hippocampus, despite high GRN levels in these tissues. We also observed a cellular infiltrate primarily composed of T cells as well as perivascular cuffing preceding the onset of hippocampal degeneration and persisting until late stages of degeneration. In addition, we detected a T cell-mediated immune response, regardless of the genetic background of the mouse injected and regardless of the AAV serotype used, as well as a direct hypertrophic effect of GRN following AAV4 delivery to ependyma cells. The consistent observation of toxicity in *GRN*-injected mice in multiple experimental settings, as well as no evidence of toxicity in any of the *eGFP*-injected control mice, strongly points to GRN overexpression as the direct cause. These data emphasize the need for caution in pursuing GRN delivery in the human CNS.

Toxicity in our study was region selective, with hippocampal neurodegeneration preceded by T cell infiltration in the case of AAV9-mediated *GRN* delivery, and severe damage to the ventricular system via ependymal hypertrophy and T cell infiltration when GRN was expressed following AAV4 transduction of ependyma. We considered various explanations for our findings, starting with serotype. The tropism of AAV9 for neurons and glia, and of AAV4 for ependymal cells, might have resulted in toxic levels of transgene expression in their target tissues. However, in contrast to GRN, EGFP delivered by either AAV9 or AAV4 vectors did not elicit a degenerative or inflammatory response. This suggests that the choice of serotype and high levels of transgene expression alone are not sufficient to explain our findings. This is supported by many others' works in which overexpression by these serotypes in a variety of null or haploinsufficient models has not led to robust immune responses.

Second, the intraventricular delivery route chosen here may have triggered immunogenicity and downstream tissue destruction. In this respect, the recent reports by Arrant et al. demonstrating rescue in mouse models of FTD and CLN11 after intraparenchymal delivery of *Grn* are noteworthy[37,38]; GRN was expressed in mice lacking one or both copies of *Grn*, but there was no dramatic hippocampal degeneration or ependymal toxicity. It is possible that the intraventricular route exposes particular antigen-presenting cells to GRN, thus provoking the T cell infiltration and inflammation observed in our animals. Our strategy was based on considerations of eventual clinical translation for *GRN*-deficient human diseases, for which intraparenchymal delivery poses safety and feasibility issues in humans. Moreover, intraventricular CNS delivery of many transgenes has been successfully achieved in preclinical models, including in animals null for the therapeutic gene. In mice, at doses and injection routes similar to ours, gene replacement strategies have consistently been safely achieved in null models; for instance, one group safely delivered the ATP-binding cassette transporter (*ABCD1*) gene in a mouse model of X-linked adrenoleukodystrophy.[39] Similarly, in our studies, overexpression of EGFP, a completely foreign protein, was well tolerated, regardless of serotype. Furthermore, MPS IIIA *Sgsh* null mice treated

was also dense hypercellularity with perivascular cuffing that was CD3+ and B220− (right box and magnifications on right; scale bars: 100 μm; n = 3 mice analyzed). (J) Rat brain slices were incubated with mouse serum from uninjected (top, n = 3), AAV9.*eGFP*-injected (second, n = 2), or AAV9.*GRN*-injected (third, n = 5) mice at 6 months post-injection, with GAD65+ mouse serum used as a positive control for antibody-based hippocampal reactivity (bottom). There was no immune reactivity in serum collected from mice injected with AAV9.*GRN* at 6 months (J) or at 1 (n = 3) or 3 (n = 2) months after AAV9.*GRN* injection (data not shown). (Scale bars: 250 μm.)

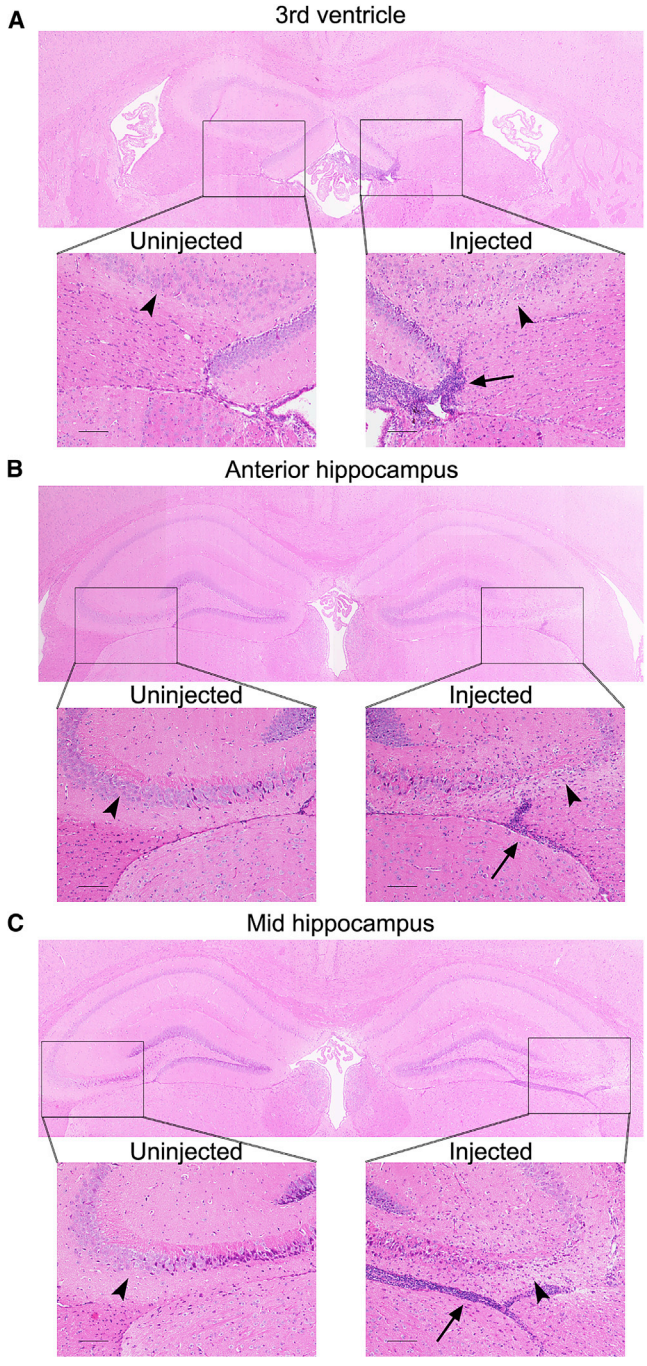

Figure 7. WT Mice Also Mount a T Cell Response Accompanied by Hippocampal Cellular Loss after Injection with AAV9.*GRN*

WT background-matched mice were injected in the right lateral ventricle at 6 months of age with AAV9.*GRN* and sacrificed at 1 (data not shown) or 3 months post-injection (n = 2 mice per time point). A hypercellular infiltrate was observed most prominently adjacent to the third ventricle ipsilateral to injection (A) and extending posteriorly throughout the anterior hippocampus (B) and mid-hippocampus (C). The infiltrate extended inferior to the hippocampus (arrows) as well as within the parenchyma, where we observed marked loss of cells in the CA2/3 region of the hippocampus on the injected side compared to the uninjected side (arrowheads; n = 1/2 mice affected at 1 month and 2/2 mice at 3 months). There was no evidence of cell loss or hypercellular infiltrate in AAV9.*eGFP*-injected WT mice (n = 2 at 3 months; data not shown). (Scale bars: 100 μm.)

with AAV4.*SGSH*, a secreted protein, using the same approach as our study, showed no sign of hippocampal or ventricular degeneration or of cellular infiltrate.[51] Cumulatively, the data suggest that our results are specific to overexpression of *GRN* as a target gene, rather than route of delivery, dose, expression of a human gene in a null mouse model, or expression of a secreted protein.

While much of the literature in more than 10 years since *GRN* mutations were first linked to neurodegeneration is concerned with the role of GRN as a neurotrophic factor,[14,16–18] *GRN* is also widely expressed in cell types ranging from epithelial cells to hematopoietic cells, macrophages, and T cells.[12,13] Early studies described its role in wound healing and regulation of inflammation, which, while poorly understood, involves an interplay between GRN, which is itself active, and its cleavage products, the granulins, which have opposing effects on a number of immune cell-mediated processes.[13] Thus, the existing literature on GRN suggests that tight regulation of its expression, both on the transcriptional side and with respect to the protein cleavage events that generate daughter peptides, may be needed to avoid untoward immunological effects.

There is also extensive literature on the involvement of GRN in cell growth and proliferation, both in normal development and in cancer.[12,13] Indeed, GRN is overexpressed and promotes cell growth in many tumors, including glioblastoma.[52,53] In this respect, our findings using AAV4-mediated *GRN* delivery are noteworthy. In mice, AAV4 selectively targets ependymal cells and subventricular astrocytes,[54] and AAV4-mediated *GRN* delivery resulted in marked hypertrophy of the ependyma, suggesting a direct effect of GRN on the targeted cells accompanied by T cell infiltration.

Arrant et al.[37,38] recently reported the reversal of phenotypes associated with *GRN* deficiency using AAV-mediated replacement therapy in *Grn* null mice, with no reported evidence of T cell infiltration or hippocampal degeneration. Despite differences in our approach (intraventricular versus intraparenchymal), vector (AAV9 or AAV4 versus AAV1), dose (higher in our study), and transgene (our vector does not have a Myc tag and can interact with sortilin), both Arrant et al. and we observed an immune response. In the case of Arrant et al., the response consists of profound microglial activation and major histocompatibility complex class II (MHCII) presentation at the injection site, as well as antibodies to GRN detected in plasma. In our studies, by contrast, we observed T cell infiltration and destruction of neurons and astrocytes in the hippocampus. It is possible that, given a longer period of time, evidence of neuronal degeneration or unchecked growth would emerge in their studies. Indeed, Arrant et al. remarked that the upregulation of MHCII is typically associated with a T cell response and speculated that a longer exposure could result in T cell-mediated neuronal degeneration and functional deficits.

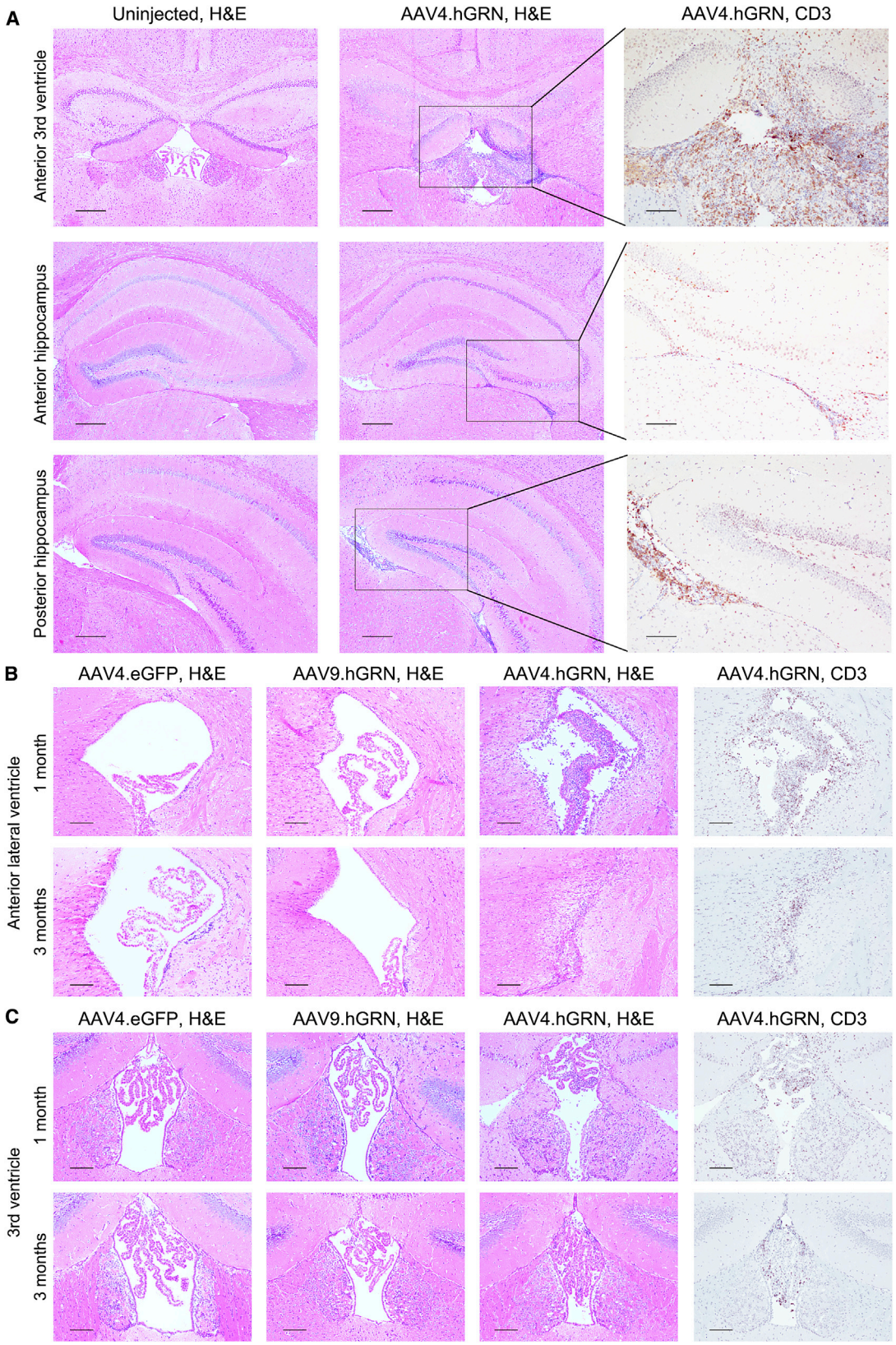

(legend on next page)

These findings raise concerns regarding how to safely translate these studies to humans. Specifically, our combined data suggest that GRN replacement could be highly immunogenic in CLN11 (*GRN* null) patients. For FTD due to haploinsufficiency, high levels of GRN may be required to reverse disease, which, in turn, may induce either tumorigenic growth effects of GRN or an immune response to transduced cells. To tease apart whether toxicity is dependent on the growth-promoting properties of GRN, overexpression in target cells, or host naiveté, additional studies are needed in heterozygous models with progranulin variants. As a final consideration, future pharmacological toxicity studies of the WT human protein may remain a challenge, as overexpression will be problematic in rodents.

In summary, while *GRN*-associated FTD and NCL are attractive targets for gene replacement therapy, our results suggest that concerns stemming from the identity and function of the transgene—*GRN*—are paramount in considerations of a path to human intervention. Specifically, work elucidating the mechanisms by which GRN modulates inflammatory and growth responses, particularly in the CNS, are needed. Our work highlights the potential for inflammatory and tumorigenic effects of *GRN* overexpression, to which specific attention should be paid in preclinical models. More broadly, these findings call into question our current conception of the brain as an immune privileged organ broadly tolerant of transgene overexpression.

MATERIALS AND METHODS

Viral Vector Constructs

AAV9 and AAV4 were used for these studies. AAV9 vectors contained a cytomegalovirus (CMV) promoter, while AAV4 vectors contained a CAG promoter. The human *GRN* cDNA (GenBank: BC000324) was amplified from a Hek293 cell cDNA library, and the mouse *Grn* cDNA (GenBank: NM_008175) was cloned using gBlocks (Integrated DNA Technologies; IDT). The transgenes or an *eGFP* reporter gene was inserted into the G0347 pFB.AAV.CMV.bHGpA plasmid or the G0347 pFB.AAV.CAG.bHGpA plasmid (Iowa Vector Core, Iowa City, IA, USA) and were then used to produce AAV vectors by the Children's Hospital of Philadelphia (CHOP) Research Vector Core (Philadelphia, PA, USA). All constructs were verified by Sanger sequencing (CHOP NAPCORE, Philadelphia, PA, USA).

Mice

Generation of progranulin null (G*rn* null) mice on a C57BL/6J background through targeted disruption of the *Grn* gene has been reported previously.[55] *Grn* null mice were provided to the University of Pennsylvania from the Nishihara laboratory at the University of Tokyo, and the colony was expanded and maintained. Male and female WT C57BL/6J (WT; Jackson Laboratories, Bar Harbor, ME, USA) and *Grn* null mice ages 6–15 months were used in these studies, as well as age-matched WT C57BL/6J controls. Mice were housed in a controlled-temperature environment on a 12-hr:12-hr light:dark cycle and were given free access to food and water. All animal studies were approved by the Institutional Animal Care and Use Committee of the University of Pennsylvania. MPS IIIA *Sgsh* null and heterozygous mice were generated and maintained as previously described,[51] and studies were approved by the Institutional Animal Care and Use Committee of CHOP.

Stereotaxic Delivery

Mice were deeply anesthetized with isoflurane and immobilized in a stereotaxic frame (David Kopf Instruments, Tujunga, CA, USA) installed with both a digital stereotaxic control panel (Leica Biosystems, Buffalo Grove, IL) and a microinjection robot (KD Scientific, Holliston, MA, USA) for motorized injections. Mice were injected unilaterally by a team of the same two operators in the posterior right lateral ventricle via a Hamilton syringe using the following coordinates: anterior-posterior (AP), −2.18 mm; medial-lateral (ML), −2.9 mm; and dorsal-ventral (DV), −3.5 mm (from bone) relative to bregma. Each mouse received 10 μL vector at a concentration of 5e+12 viral genomes per milliliter (vg/mL), for a total dose of 5e+10 vg, with the exception of AAV4.*eGFP*, which was delivered at a concentration of 4e+11 vg/mL, for a total dose of 4e+9 vg. Vectors were infused at a rate of 0.5 μL/min, with a 3-min wait time post-infusion prior to withdrawal of the trochanter. All vector dilutions were prepared in parallel using the same diluent, and experimental and control mice were injected on the same day in a mixed order. Mice were injected between 6 and 8 months of age and euthanized between 1 and 9 months post-injection. MPS IIIA *Sgsh* null and heterozygous mice were injected at 2 months and euthanized at 5.5 months, as previously described.[51]

Mouse Brain Isolation

Mice were sacrificed at indicated ages by anesthetizing with a ketamine-xylazine-acepromazine mixture, followed by transcardial perfusion with 15 mL ice-cold 0.9% PBS. Brains were quickly removed from the skull. Those used for fluorescent imaging studies were fixed whole in 4% paraformaldehyde overnight at 4°C followed by placement in a 30% sucrose-0.05% sodium azide solution for cryoprotection at 4°C. Those used for immunohistochemistry or for GRN

Figure 8. *Grn* Null Mice Expressing GRN Delivered by an Ependymal-Targeting Vector, AAV4, Show an Inflammatory Response and Ependymal Hypertrophy
Mice were injected at 6.5–8 months of age in the right lateral ventricle with AAV4.*GRN* and sacrificed 1 or 3 months post-injection. At 1 month, AAV4.*GRN*-injected mice showed a dense cellular infiltrate throughout the ependyma underlying the hippocampus (A, middle panels) that was not present in uninjected age-matched controls (A, left panels) or in AAV4.*eGFP*-injected littermates (data not shown). (Scale bars: 250 μm.) The infiltrate was highly positive for the T cell marker CD3 in all regions (A, right panels; scale bars: 100 μm). When compared to age-matched AAV9.*GRN*-injected mice, AAV4.*GRN*-injected mice showed unique choroidal and ependymal hyperplasia and thickening and dense T cell infiltration in the ipsilateral (B) and contralateral (data not shown) lateral ventricles that worsened with time to the point of effacement by 3 months post-injection (scale bars: 100 μm). This was also apparent in the third ventricle, where the ependyma were thickened and the choroid nearly filled the ventricle by 3 months, again with a T cell infiltrate (C; scale bars: 100 μm). 3/3 AAV4.*GRN*-injected mice were affected at each of the 1- and 3-month post-injection time points, while AAV4.*eGFP* control brains were not affected (n = 2 at 1 month, and n = 1 at 3 months).

quantification by ELISA were blocked into 2-mm-thick coronal slices and then either fixed in 4% paraformaldehyde overnight at 4°C or microdissected and flash-frozen in liquid nitrogen, respectively.

Protein Extraction

Frozen isolated brain tissues were weighed, transferred to a 500-μL Potter-Elvehjem Dounce homogenizer (Sigma-Aldrich, Allentown, PA, USA), and manually homogenized in 1% radioimmunoprecipitation buffer (RIPA buffer; 50 mM Tris, 150 mM NaCl, 5 mM EDTA, 0.5% sodium deoxycholate, 1% NP-40, and 0.1% SDS [pH 8.0]) with 0.2% PMSF and 0.1% protease inhibitors (Penn Center for Neurodegenerative Research [CNDR], Philadelphia, PA, USA). Homogenates were centrifuged at 21,380 × *g* RCF for 30 min, supernatant was harvested, and protein concentration was measured by the Pierce BCA Protein Assay (Thermo Fisher Scientific, Waltham, MA, USA). GRN was quantified by using a human progranulin ELISA kit (Adipogen, San Diego, CA, USA). 118 μg total protein was plated per well, with samples run in duplicate. Plates were read on a TriStar vTI LB 941 multimode reader (Berthold Technologies, Bad Wildbad, Germany) at a wavelength of 450 nm, and GRN concentration was calculated using the provided standard curve per kit instructions. Graphs were prepared using GraphPad Prism Version 7.00c for MacOS X and GraphPad software (La Jolla, CA, USA; www.graphpad.com).

Antibodies

Primary antibodies used for immunohistochemistry included the following: anti-human GRN rabbit polyclonal antibody (0.01 mg/mL; developed by CNDR, Philadelphia, PA, USA, as previously described[15]), anti-NeuN rabbit polyclonal antibody (0.5 μg/mL; ABN78; Sigma-Aldrich, St. Louis, MO, USA), anti-GFAP rabbit polyclonal antibody (0.58 μg/mL; Z0334; Dako-Agilent, Santa Clara, CA, USA), anti-Iba1 rabbit polyclonal antibody (0.25 μg/mL; Saf5299; Wako Pure Chemical Industries, Richmond, VA), anti-Ki67 rabbit monoclonal antibody (dilution 1:1,000; ab16667; Abcam, Cambridge, UK), anti-CD45R rat monoclonal antibody (5 μg/mL; RA3-6B2; Invitrogen, Carlsbad, CA, USA), and anti-CD3e rabbit monoclonal antibody (dilution 1:150; MA1-90582; Invitrogen, Carlsbad, CA, USA). Biotinylated goat anti-rabbit and goat anti-rat immunoglobulin G (IgG) secondary antibodies (Vector Laboratories, Burlingame, CA, USA) was used at a concentration of 1.5 μg/mL in all cases except for anti-GRN, for which the secondary antibody concentration was 7.5 μg/mL. In the autoantibody studies, biotinylated goat anti-mouse IgG secondary antibody (Vector Laboratories, Burlingame, CA, USA) was used at a concentration of 0.75 μg/mL.

Section Preparation and Immunohistochemistry

Fixed coronal brain slices were serially ethanol dehydrated and paraffin embedded. Blocks were sectioned coronally at 6 μm and incubated at 37–42°C overnight. Sections were deparaffinized in xylene and rehydrated in serially dilute ethanol solutions, and they either were stained with H&E (Thermo Scientific, Kalamazoo, MI, USA; and Fisher Chemical, Waltham, MA, USA) or underwent immunohistochemical (IHC) staining as follows: sections underwent deactivation of endogenous peroxidase with 5% hydrogen peroxide in methanol for 30 min as well as microwave antigen retrieval using antigen unmasking solution (Vector Laboratories, Burlingame, CA, USA), followed by washing in Tris buffer then blocking against nonspecific binding sites with 2% fetal bovine serum for 30 min at room temperature. Sections were then incubated in primary antibody overnight at 4°C in humidified chambers, blocked again, and incubated in biotinylated secondary antibody for 1 hr at room temperature. Sections were again blocked, followed by treatment for 1 hr with the VECTASTAIN ABC Kit (Vector Laboratories, Burlingame, CA, USA) for avidin binding and peroxidation, and then treated with Vector ImmPACT 3,3′-diaminobenzidine (DAB) peroxidase substrate solution for detection (Vector Laboratories, Burlingame, CA, USA). Sections were counterstained with hematoxylin and dehydrated prior to coverslipping. Bright-field images were taken on a Nikon 80i upright fluorescence microscope and analyzed with Nikon NIS-Elements AR Imaging software.

Quantitation of Hippocampal Toxicity

A 4-point scoring system was developed for rating the degree of hippocampal toxicity, with 0 representing normal hippocampus, 1 representing presence of infiltrate without cell loss, 2 representing focal cell loss, and 3 representing pervasive cell loss (Figure S5). Five evaluators experienced in mouse brain histopathology were presented with an anterior and a posterior H&E-stained slide from each mouse and were blinded with regard to time point and treatment. Each evaluator independently assigned each animal a score ranging from 0 to 4, using the scale described as a reference, and an average score was computed for each mouse. These scores were then averaged for each treatment group at each time point and plotted along with the SEM. Graphs were prepared using GraphPad Prism Version 7.00c for Mac OS X and GraphPad software (La Jolla, CA, USA; www.graphpad.com).

Section Preparation and Fluorescence Imaging

Fixed, cryoprotected brains were sectioned at 60 μm on a freezing microtome and stored at −20°C in a cryoprotectant solution (30% ethylene glycol, 15% sucrose, 0.05% sodium azide in PBS) until use. Sections were imaged using a DM6000B Leica microscope equipped with a Hamamatsu ORCA-Flash 4.0 camera.

Autoantibody Detection

Studies were performed as previously described.[56] Adult female Wistar rats were anesthetized and decapitated. Brains were removed and washed in 1× PBS and then bisected sagitally and fixed in 4% paraformaldehyde in PBS at 4°C for 1 hr. Brains were then transferred to 40% sucrose in 0.1 M PBS for 48 hr, followed by embedding in Tissue-Tek O.C.T. Compound embedding medium (Sakura Finitek, Torrance, CA, USA), and then snap-frozen in 2-methylbutane cooled with liquid nitrogen. Sections were cut sagitally at 7 μm, mounted on glass slides, and stored at −20°C until use. Endogenous peroxidase was quenched with 0.3% hydrogen peroxide in PBS for 15 min. Sections were blocked in 5% goat normal serum for 1 hr, after which serum samples were applied to sections at a dilution of 1:200 in 5% normal goat serum (Jackson ImmunoResearch Laboratories, West Grove, PA, USA) and incubated overnight at 4°C in humidified

chambers. Sections were incubated in biotinylated goat anti-mouse secondary antibody for 2 hr at room temperature and then were treated for 1 hr with the VECTASTAIN Elite ABC Kit (Vector Laboratories, Burlingame, CA, USA) for avidin binding and peroxidation. Slides were incubated for 30 s in 0.5% Triton X solution in PBS and then treated with the Vector ImmPACT DAB peroxidase substrate kit (Vector Laboratories, Burlingame, CA, USA) for detection. Slides were counterstained with 50% hematoxylin and dehydrated prior to coverslipping. Bright-field images were taken on a Nikon 80i upright fluorescence microscope and analyzed with Nikon NIS-Elements AR Imaging software.

SUPPLEMENTAL INFORMATION

Supplemental Information includes five figures and one table and can be found with this article online at https://doi.org/10.1016/j.ymthe.2018.11.013.

AUTHOR CONTRIBUTIONS

Conceptualization, A.S.C.-P., B.L.D., D.A.A., and J.M.R.; Methodology, A.S.C.-P., B.L.D., D.A.A., J.M.R., and E.L.; Investigation, D.A.A., J.M.R., F.D., P.H.-C., A.S., J.T.M., and J.Z.; Writing – Original Draft, D.A.A. and J.M.R.; Writing – Review & Editing, A.S.C.-P., B.L.D., D.A.A., J.M.R., J.Z., J.T.M., and E.L.; Funding Acquisition, A.S.C.-P., B.L.D., and D.A.A.; Resources and Supervision, A.S.C.-P. and B.L.D.

CONFLICTS OF INTEREST

The authors declare no competing interests.

ACKNOWLEDGMENTS

We thank Masugi Nishihara for providing us with *Grn* null animals and Virginia Lee for providing GRN antibody reagents. Sources of support for this project include the Pechenik Montague Award Fund (to A.S.C.-P.), the Benaroya Award Fund (to A.S.C.-P.), and a Brody Family Medical Trust Fund fellowship (to D.A.A.).

REFERENCES

1. Baker, M., Mackenzie, I.R., Pickering-Brown, S.M., Gass, J., Rademakers, R., Lindholm, C., Snowden, J., Adamson, J., Sadovnick, A.D., Rollinson, S., et al. (2006). Mutations in progranulin cause tau-negative frontotemporal dementia linked to chromosome 17. Nature *442*, 916–919.

2. Cruts, M., Gijselinck, I., van der Zee, J., Engelborghs, S., Wils, H., Pirici, D., Rademakers, R., Vandenberghe, R., Dermaut, B., Martin, J.J., et al. (2006). Null mutations in progranulin cause ubiquitin-positive frontotemporal dementia linked to chromosome 17q21. Nature *442*, 920–924.

3. Smith, K.R., Damiano, J., Franceschetti, S., Carpenter, S., Canafoglia, L., Morbin, M., Rossi, G., Pareyson, D., Mole, S.E., Staropoli, J.F., et al. (2012). Strikingly different clinicopathological phenotypes determined by progranulin-mutation dosage. Am. J. Hum. Genet. *90*, 1102–1107.

4. Grossman, M. (2002). Frontotemporal dementia: a review. J. Int. Neuropsychol. Soc. *8*, 566–583.

5. Chen-Plotkin, A.S., Martinez-Lage, M., Sleiman, P.M., Hu, W., Greene, R., Wood, E.M., Bing, S., Grossman, M., Schellenberg, G.D., Hatanpaa, K.J., et al. (2011). Genetic and clinical features of progranulin-associated frontotemporal lobar degeneration. Arch. Neurol. *68*, 488–497.

6. Canafoglia, L., Morbin, M., Scaioli, V., Pareyson, D., D'Incerti, L., Fugnanesi, V., Tagliavini, F., Berkovic, S.F., and Franceschetti, S. (2014). Recurrent generalized seizures, visual loss, and palinopsia as phenotypic features of neuronal ceroid lipofuscinosis due to progranulin gene mutation. Epilepsia *55*, e56–e59.

7. Almeida, M.R., Macário, M.C., Ramos, L., Baldeiras, I., Ribeiro, M.H., and Santana, I. (2016). Portuguese family with the co-occurrence of frontotemporal lobar degeneration and neuronal ceroid lipofuscinosis phenotypes due to progranulin gene mutation. Neurobiol. Aging *41*, 200.e1–200.e5.

8. Kousi, M., Lehesjoki, A.E., and Mole, S.E. (2012). Update of the mutation spectrum and clinical correlations of over 360 mutations in eight genes that underlie the neuronal ceroid lipofuscinoses. Hum. Mutat. *33*, 42–63.

9. Capell, A., Liebscher, S., Fellerer, K., Brouwers, N., Willem, M., Lammich, S., Gijselinck, I., Bittner, T., Carlson, A.M., Sasse, F., et al. (2011). Rescue of progranulin deficiency associated with frontotemporal lobar degeneration by alkalizing reagents and inhibition of vacuolar ATPase. J. Neurosci. *31*, 1885–1894.

10. Cenik, B., Sephton, C.F., Dewey, C.M., Xian, X., Wei, S., Yu, K., Niu, W., Coppola, G., Coughlin, S.E., Lee, S.E., et al. (2011). Suberoylanilide hydroxamic acid (vorinostat) up-regulates progranulin transcription: rational therapeutic approach to frontotemporal dementia. J. Biol. Chem. *286*, 16101–16108.

11. Lee, W.C., Almeida, S., Prudencio, M., Caulfield, T.R., Zhang, Y.J., Tay, W.M., Bauer, P.O., Chew, J., Sasaguri, H., Jansen-West, K.R., et al. (2014). Targeted manipulation of the sortilin-progranulin axis rescues progranulin haploinsufficiency. Hum. Mol. Genet. *23*, 1467–1478.

12. Toh, H., Chitramuthu, B.P., Bennett, H.P., and Bateman, A. (2011). Structure, function, and mechanism of progranulin; the brain and beyond. J. Mol. Neurosci. *45*, 538–548.

13. Jian, J., Konopka, J., and Liu, C. (2013). Insights into the role of progranulin in immunity, infection, and inflammation. J. Leukoc. Biol. *93*, 199–208.

14. Petkau, T.L., Neal, S.J., Orban, P.C., MacDonald, J.L., Hill, A.M., Lu, G., Feldman, H.H., Mackenzie, I.R., and Leavitt, B.R. (2010). Progranulin expression in the developing and adult murine brain. J. Comp. Neurol. *518*, 3931–3947.

15. Chen-Plotkin, A.S., Xiao, J., Geser, F., Martinez-Lage, M., Grossman, M., Unger, T., Wood, E.M., Van Deerlin, V.M., Trojanowski, J.Q., and Lee, V.M. (2010). Brain progranulin expression in GRN-associated frontotemporal lobar degeneration. Acta Neuropathol. *119*, 111–122.

16. Van Damme, P., Van Hoecke, A., Lambrechts, D., Vanacker, P., Bogaert, E., van Swieten, J., Carmeliet, P., Van Den Bosch, L., and Robberecht, W. (2008). Progranulin functions as a neurotrophic factor to regulate neurite outgrowth and enhance neuronal survival. J. Cell Biol. *181*, 37–41.

17. Gao, X., Joselin, A.P., Wang, L., Kar, A., Ray, P., Bateman, A., Goate, A.M., and Wu, J.Y. (2010). Progranulin promotes neurite outgrowth and neuronal differentiation by regulating GSK-3β. Protein Cell *1*, 552–562.

18. Beel, S., Moisse, M., Damme, M., De Muynck, L., Robberecht, W., Van Den Bosch, L., Saftig, P., and Van Damme, P. (2017). Progranulin functions as a cathepsin D chaperone to stimulate axonal outgrowth in vivo. Hum. Mol. Genet. *26*, 2850–2863.

19. Hu, F., Padukkavidana, T., Vægter, C.B., Brady, O.A., Zheng, Y., Mackenzie, I.R., Feldman, H.H., Nykjaer, A., and Strittmatter, S.M. (2010). Sortilin-mediated endocytosis determines levels of the frontotemporal dementia protein, progranulin. Neuron *68*, 654–667.

20. Minami, S.S., Min, S.W., Krabbe, G., Wang, C., Zhou, Y., Asgarov, R., Li, Y., Martens, L.H., Elia, L.P., Ward, M.E., et al. (2014). Progranulin protects against amyloid β deposition and toxicity in Alzheimer's disease mouse models. Nat. Med. *20*, 1157–1164.

21. Van Kampen, J.M., and Kay, D.G. (2017). Progranulin gene delivery reduces plaque burden and synaptic atrophy in a mouse model of Alzheimer's disease. PLoS ONE *12*, e0182896.

22. Van Kampen, J.M., Baranowski, D., and Kay, D.G. (2014). Progranulin gene delivery protects dopaminergic neurons in a mouse model of Parkinson's disease. PLoS ONE *9*, e97032.

23. Laird, A.S., Van Hoecke, A., De Muynck, L., Timmers, M., Van den Bosch, L., Van Damme, P., and Robberecht, W. (2010). Progranulin is neurotrophic in vivo and protects against a mutant TDP-43 induced axonopathy. PLoS ONE *5*, e13368.

24. Chitramuthu, B.P., Kay, D.G., Bateman, A., and Bennett, H.P. (2017). Neurotrophic effects of progranulin in vivo in reversing motor neuron defects caused by over or under expression of TDP-43 or FUS. PLoS ONE *12*, e0174784.

25. Tauffenberger, A., Chitramuthu, B.P., Bateman, A., Bennett, H.P., and Parker, J.A. (2013). Reduction of polyglutamine toxicity by TDP-43, FUS and progranulin in Huntington's disease models. Hum. Mol. Genet. *22*, 782–794.

26. Russell, S., Bennett, J., Wellman, J.A., Chung, D.C., Yu, Z.F., Tillman, A., Wittes, J., Pappas, J., Elci, O., McCague, S., et al. (2017). Efficacy and safety of voretigene neparvovec (AAV2-hRPE65v2) in patients with RPE65-mediated inherited retinal dystrophy: a randomised, controlled, open-label, phase 3 trial. Lancet *390*, 849–860.

27. Dunbar, C.E., High, K.A., Joung, J.K., Kohn, D.B., Ozawa, K., and Sadelain, M. (2018). Gene therapy comes of age. Science *359*, eaan4672.

28. Mendell, J.R., Al-Zaidy, S., Shell, R., Arnold, W.D., Rodino-Klapac, L.R., Prior, T.W., Lowes, L., Alfano, L., Berry, K., Church, K., et al. (2017). Single-dose gene-replacement therapy for spinal muscular atrophy. N. Engl. J. Med. *377*, 1713–1722.

29. Sands, M.S., and Davidson, B.L. (2006). Gene therapy for lysosomal storage diseases. Mol. Ther. *13*, 839–849.

30. Katz, M.L., Tecedor, L., Chen, Y., Williamson, B.G., Lysenko, E., Wininger, F.A., Young, W.M., Johnson, G.C., Whiting, R.E., Coates, J.R., and Davidson, B.L. (2015). AAV gene transfer delays disease onset in a TPP1-deficient canine model of the late infantile form of Batten disease. Sci. Transl. Med. *7*, 313ra180.

31. Chen, Y.H., Chang, M., and Davidson, B.L. (2009). Molecular signatures of disease brain endothelia provide new sites for CNS-directed enzyme therapy. Nat. Med. *15*, 1215–1218.

32. Monteys, A.M., Ebanks, S.A., Keiser, M.S., and Davidson, B.L. (2017). CRISPR/Cas9 editing of the mutant huntingtin allele in vitro and in vivo. Mol. Ther. *25*, 12–23.

33. Meyer, K., Ferraiuolo, L., Schmelzer, L., Braun, L., McGovern, V., Likhite, S., Michels, O., Govoni, A., Fitzgerald, J., Morales, P., et al. (2015). Improving single injection CSF delivery of AAV9-mediated gene therapy for SMA: a dose-response study in mice and nonhuman primates. Mol. Ther. *23*, 477–487.

34. Haurigot, V., Marcó, S., Ribera, A., Garcia, M., Ruzo, A., Villacampa, P., Ayuso, E., Añor, S., Andaluz, A., Pineda, M., et al. (2013). Whole body correction of mucopolysaccharidosis IIIA by intracerebrospinal fluid gene therapy. J. Clin. Invest. *123*, 3254–3271.

35. Mingozzi, F., and High, K.A. (2017). Overcoming the host immune response to adeno-associated virus gene delivery vectors: the race between clearance, tolerance, neutralization, and escape. Annu. Rev. Virol. *4*, 511–534.

36. Vandamme, C., Adjali, O., and Mingozzi, F. (2017). Unraveling the complex story of immune responses to AAV vectors trial after trial. Hum. Gene Ther. *28*, 1061–1074.

37. Arrant, A.E., Onyilo, V.C., Unger, D.E., and Roberson, E.D. (2018). Progranulin gene therapy improves lysosomal dysfunction and microglial pathology associated with frontotemporal dementia and neuronal ceroid lipofuscinosis. J. Neurosci. *38*, 2341–2358.

38. Arrant, A.E., Filiano, A.J., Unger, D.E., Young, A.H., and Roberson, E.D. (2017). Restoring neuronal progranulin reverses deficits in a mouse model of frontotemporal dementia. Brain *140*, 1447–1465.

39. Gong, Y., Mu, D., Prabhakar, S., Moser, A., Musolino, P., Ren, J., Breakefield, X.O., Maguire, C.A., and Eichler, F.S. (2015). Adenoassociated virus serotype 9-mediated gene therapy for X-linked adrenoleukodystrophy. Mol. Ther. *23*, 824–834.

40. Liu, G., Martins, I., Wemmie, J.A., Chiorini, J.A., and Davidson, B.L. (2005). Functional correction of CNS phenotypes in a lysosomal storage disease model using adeno-associated virus type 4 vectors. J. Neurosci. *25*, 9321–9327.

41. Dodge, J.C., Treleaven, C.M., Fidler, J.A., Hester, M., Haidet, A., Handy, C., Rao, M., Eagle, A., Matthews, J.C., Taksir, T.V., et al. (2010). AAV4-mediated expression of IGF-1 and VEGF within cellular components of the ventricular system improves survival outcome in familial ALS mice. Mol. Ther. *18*, 2075–2084.

42. Ahmed, Z., Sheng, H., Xu, Y.F., Lin, W.L., Innes, A.E., Gass, J., Yu, X., Wuertzer, C.A., Hou, H., Chiba, S., et al. (2010). Accelerated lipofuscinosis and ubiquitination in granulin knockout mice suggest a role for progranulin in successful aging. Am. J. Pathol. *177*, 311–324.

43. Wils, H., Kleinberger, G., Pereson, S., Janssens, J., Capell, A., Van Dam, D., Cuijt, I., Joris, G., De Deyn, P.P., Haass, C., et al. (2012). Cellular ageing, increased mortality and FTLD-TDP-associated neuropathology in progranulin knockout mice. J. Pathol. *228*, 67–76.

44. Ghoshal, N., Dearborn, J.T., Wozniak, D.F., and Cairns, N.J. (2012). Core features of frontotemporal dementia recapitulated in progranulin knockout mice. Neurobiol. Dis. *45*, 395–408.

45. Sofroniew, M.V., and Vinters, H.V. (2010). Astrocytes: biology and pathology. Acta Neuropathol. *119*, 7–35.

46. Lancaster, E., Martinez-Hernandez, E., Titulaer, M.J., Boulos, M., Weaver, S., Antoine, J.C., Liebers, E., Kornblum, C., Bien, C.G., Honnorat, J., et al. (2011). Antibodies to metabotropic glutamate receptor 5 in the Ophelia syndrome. Neurology *77*, 1698–1701.

47. Lancaster, E., and Dalmau, J. (2012). Neuronal autoantigens–pathogenesis, associated disorders and antibody testing. Nat. Rev. Neurol. *8*, 380–390.

48. Foust, K.D., Nurre, E., Montgomery, C.L., Hernandez, A., Chan, C.M., and Kaspar, B.K. (2009). Intravascular AAV9 preferentially targets neonatal neurons and adult astrocytes. Nat. Biotechnol. *27*, 59–65.

49. Davidson, B.L., Stein, C.S., Heth, J.A., Martins, I., Kotin, R.M., Derksen, T.A., Zabner, J., Ghodsi, A., and Chiorini, J.A. (2000). Recombinant adeno-associated virus type 2, 4, and 5 vectors: transduction of variant cell types and regions in the mammalian central nervous system. Proc. Natl. Acad. Sci. USA *97*, 3428–3432.

50. Hudry, E., Dashkoff, J., Roe, A.D., Takeda, S., Koffie, R.M., Hashimoto, T., Scheel, M., Spires-Jones, T., Arbel-Ornath, M., Betensky, R., et al. (2013). Gene transfer of human *Apoe* isoforms results in differential modulation of amyloid deposition and neurotoxicity in mouse brain. Sci. Transl. Med. *5*, 212ra161.

51. Chen, Y., Zheng, S., Tecedor, L., and Davidson, B.L. (2018). Overcoming limitations inherent in sulfamidase to improve mucopolysaccharidosis IIIA gene therapy. Mol. Ther. *26*, 1118–1126.

52. Liau, L.M., Lallone, R.L., Seitz, R.S., Buznikov, A., Gregg, J.P., Kornblum, H.I., Nelson, S.F., and Bronstein, J.M. (2000). Identification of a human glioma-associated growth factor gene, granulin, using differential immuno-absorption. Cancer Res. *60*, 1353–1360.

53. Menges, C.W., Chen, Y., Mossman, B.T., Chernoff, J., Yeung, A.T., and Testa, J.R. (2010). A Phosphotyrosine proteomic screen identifies multiple tyrosine kinase signaling pathways aberrantly activated in malignant mesothelioma. Genes Cancer *1*, 493–505.

54. Liu, G., Martins, I.H., Chiorini, J.A., and Davidson, B.L. (2005). Adeno-associated virus type 4 (AAV4) targets ependyma and astrocytes in the subventricular zone and RMS. Gene Ther. *12*, 1503–1508.

55. Kayasuga, Y., Chiba, S., Suzuki, M., Kikusui, T., Matsuwaki, T., Yamanouchi, K., Kotaki, H., Horai, R., Iwakura, Y., and Nishihara, M. (2007). Alteration of behavioural phenotype in mice by targeted disruption of the progranulin gene. Behav. Brain Res. *185*, 110–118.

56. McCracken, L., Zhang, J., Greene, M., Crivaro, A., Gonzalez, J., Kamoun, M., and Lancaster, E. (2017). Improving the antibody-based evaluation of autoimmune encephalitis. Neurol. Neuroimmunol. Neuroinflamm. *4*, e404.

YMTHE, Volume *27*

Supplemental Information

AAV-Mediated Progranulin Delivery to a Mouse Model of Progranulin Deficiency Causes T Cell-Mediated Toxicity

Defne A. Amado, Julianne M. Rieders, Fortunay Diatta, Pilar Hernandez-Con, Adina Singer, Jordan T. Mak, Junxian Zhang, Eric Lancaster, Beverly L. Davidson, and Alice S. Chen-Plotkin

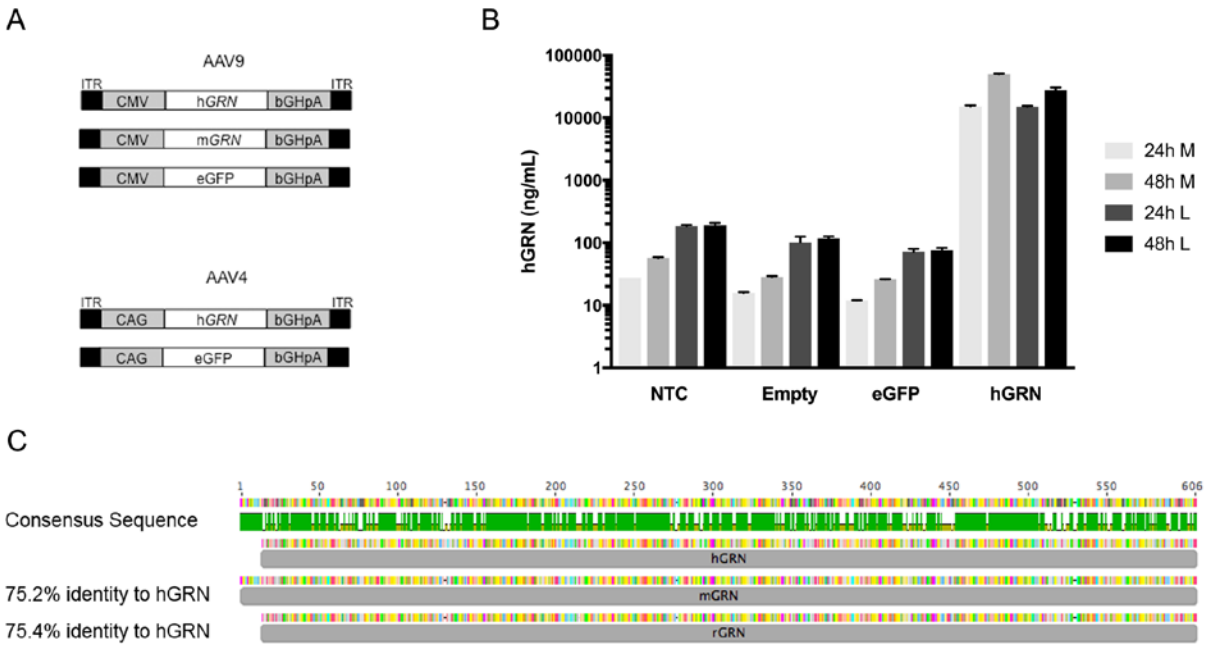

Fig. S1. (A) Schematic of AAV transgene cassettes used in our experiments. For AAV9 vectors, the CMV promoter was used to drive human progranulin (*GRN*), mouse progranulin (*Grn*), or enhanced green fluorescent protein (*eGFP*), followed by the bovine growth hormone polyA (bGHpA), and flanked by AAV2 inverted terminal repeats (ITR). For AAV4 the CAG promoter was used to drive *GRN* or *eGFP*, followed by the bovine growth hormone polyA (bGHpA), flanked by the AAV2 inverted terminal repeats (ITR). (B) Plasmid expression was validated by transfection of HEK293 cells (QBI) with lipofectamine 2000 and measuring hGRN (shown above) or mGRN (data not shown) levels by ELISA in the media or lysate, 24 or 48 hours after transfection as indicated. Our expression plasmids are compared to non-transfected cells (NTC), cells transfected with the empty vector (5/TO) or *eGFP* transfected cells. Levels were similar between hGRN and mGRN. (C) Schematic of hGRN, mGRN, and rat GRN (rGRN) protein consensus and alignments. rGRN and mGRN share 75.4% and 75.2% identity to hGRN respectively. Alignment and figure were generated using Geneious 7.1.7 (https://www.geneious.com).

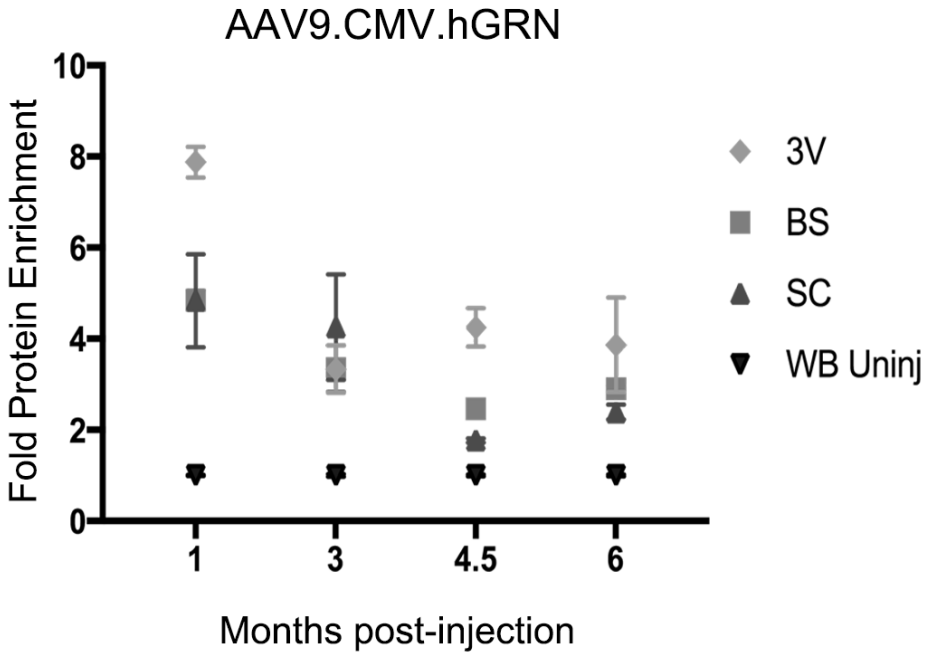

Fig. S2. AAV9 mediates *GRN* expression in *Grn* null mouse brain. *Grn* null mice were injected at 6-7.5 months of age with AAV9.*GRN* in the right lateral ventricle and sacrificed 1- , 3- , 4.5- , or 6 months post-injection. Brains were microdissected and GRN levels measured by ELISA. GRN levels in the third peri-ventricular area (3V), brain stem (BS), and spinal cord (SC) were elevated at all time points compared to uninjected homogenized whole brain (WB). *n* = 3 mice/group at each time point.

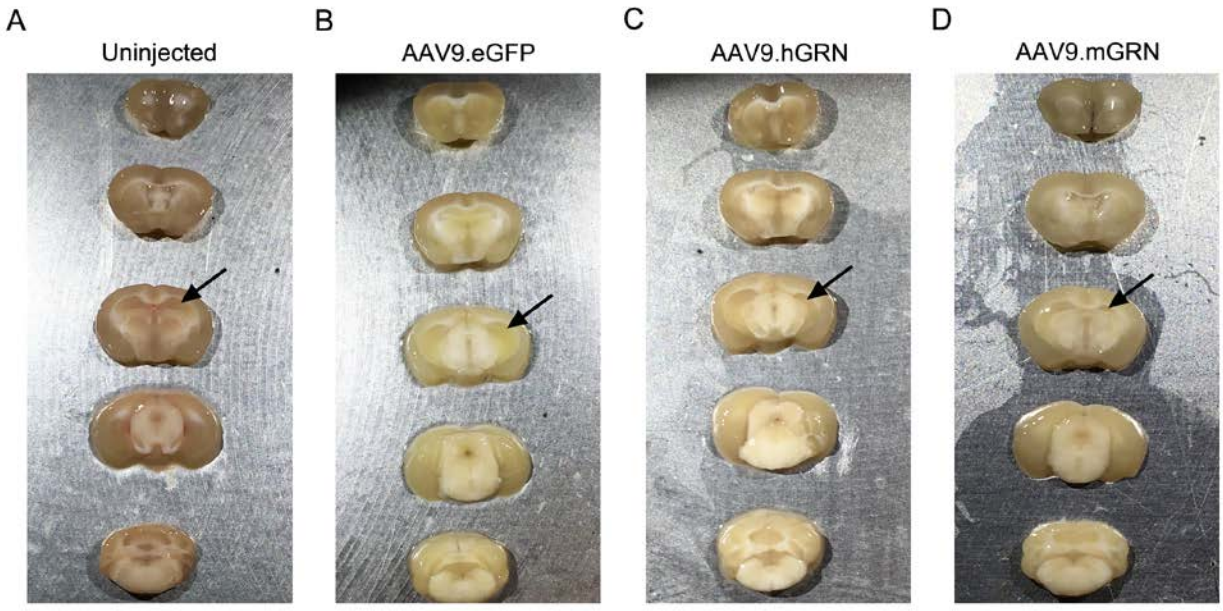

Fig. S3. Gross morphological changes are observed in AAV9.*GRN*- and AAV9.*Grn*-injected *Grn* null mice. Mice were injected with AAV9.*GRN*, AAV9.*Grn*, or AAV9.*eGFP* at 6-7.5 months of age and sacrificed 6 months post-injection. Brains were cut into 2mm sections prior to microdissection. While uninjected (A) and AAV9.*eGFP*-injected (B) mice show no overt morphological differences, the injected (right) hemisphere of mice treated with AAV9.*GRN* (C) and AAV9.*Grn* (D) was noticeably smaller, specifically in the hippocampal region (arrows), with surrounding regions appearing unaffected. n = 10 mice treated with AAV9.*GRN* (6 grossly affected and remainder affected when assessed histologically), n = 3 mice treated with AAV9.*Grn* (3 grossly affected), n = 4 mice treated with AAV9.*eGFP* (0 affected), n = 4 mice uninjected (0 affected).

A

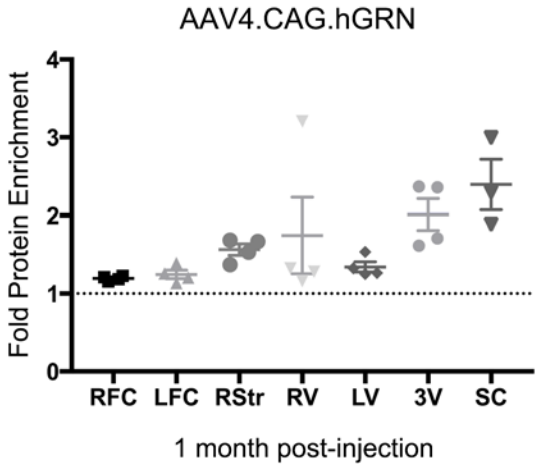

Fig. S4. AAV4 mediates *GRN* expression and toxicity in ependyma-rich areas of *Grn* null mouse brain. *Grn* null mice were injected at 6-9 months of age with AAV4.*GRN* in the right lateral ventricle. (A) Brains were microdissected 1 month post-injection and GRN levels were measured by ELISA. GRN levels in the right and left frontal cortex (RFC, LFC), right striatum (RStr), right and left peri-ventricular area (RV, LV), third ventricle (3V), and spinal cord (SC) were measured, with uninjected whole brain represented by a dotted line. A small increase in expression was seen that was most pronounced in regions with a high ependymal content, such as RV, 3V and SC. (*n* = 3 mice/group.) (B) Mice were sacrificed 3 months post-injection and analyzed by immunohistochemistry. In the ependyma and choroid of the lateral ventricle (side panels, scale bar: 100 µm), GRN levels were increased (inset, scale bar: 25 µm) with a T cell infiltrate (CD3) and hypertrophy, while in hippocampal parenchyma (bottom panels, scale bars: 100 µm), no GRN expression or infiltrate was seen and tissue morphology was intact (*n* = 3.)

B

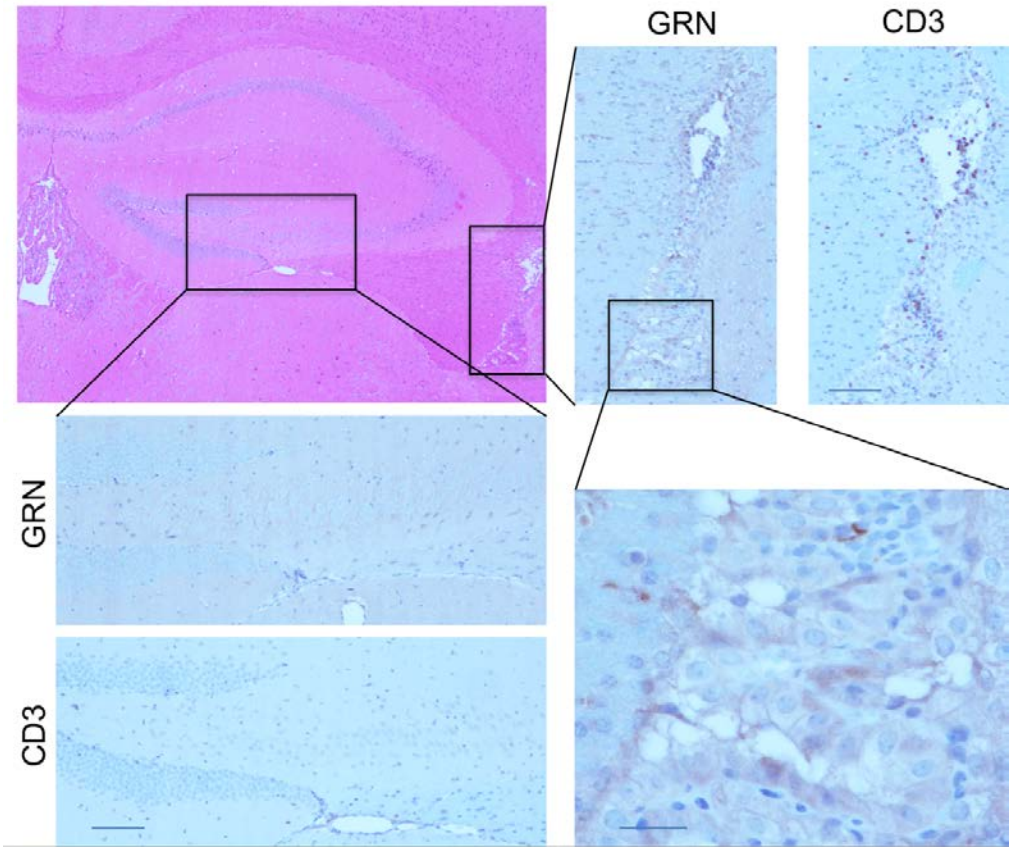
GRN
CD3
GRN
CD3

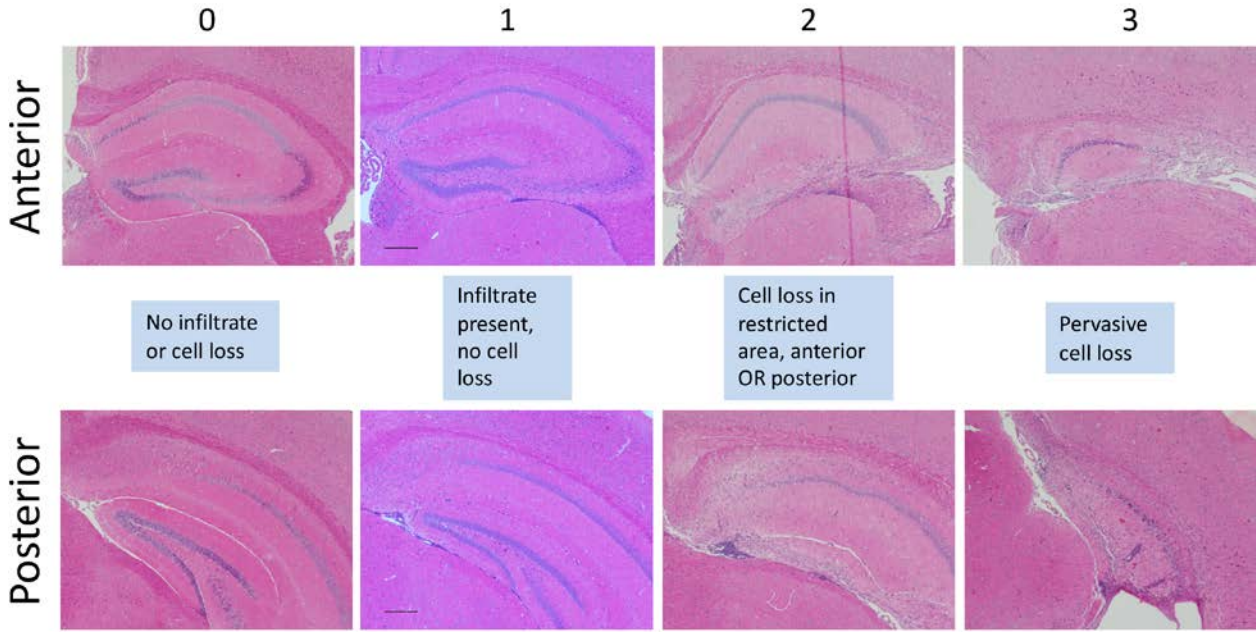
0
1
2
3
Anterior
Posterior
No infiltrate or cell loss
Infiltrate present, no cell loss
Cell loss in restricted area, anterior OR posterior
Pervasive cell loss

Fig. S5. Hippocampal pathology for AAV9.*GRN* or AAV9.*eGFP*-treated mice was assessed using a rating scale. A score of 0 was given if no pathology was seen. A score of 1 indicated that a hypercellular infiltrate was present but there was no cell loss. A score of 2 indicated cellular loss but in a restricted area, whether anterior only, posterior only, or throughout but affecting a small portion of the hippocampus. A score of 3 indicated pervasive cell loss affecting a large portion of the hippocampus. Reviewers were first trained using this scale and then presented with an anterior and a posterior image for each mouse. Each reviewer assigned a score based on observed pathology and was blinded with regards to treatment or time post-injection.

AAV9	1 month	3 months	6 months	9 months	AAV4	1 month	3 months
AAV9.*hGRN*	3/3	2/2	10/10	2/2	**AAV4.*hGRN***	3/3	3/3
AAV9.*eGFP*	0/3	0/6	0/5	0/4	**AAV4.*eGFP***	0/2	0/1

Table S1. Overview of studies performed in GRN null mice. Numerator represents number of affected mice. Denominator represents number of treated mice at each time point. All *GRN*-treated mice at all time points were affected, while no *eGFP*-treated mice were affected.